



**HAL**  
open science

## Exposure to atmospheric Ag, TiO<sub>2</sub>, Ti and SiO<sub>2</sub> engineered nanoparticles modulates gut inflammatory response and microbiota in mice

Eva Guilloteau, Madjid Djouina, Ségolène Caboche, Christophe Waxin, Karine Deboudt, Delphine Beury, David Hot, Muriel Pichavant, Laurent Dubuquoy, David Launay, et al.

### ► To cite this version:

Eva Guilloteau, Madjid Djouina, Ségolène Caboche, Christophe Waxin, Karine Deboudt, et al.. Exposure to atmospheric Ag, TiO<sub>2</sub>, Ti and SiO<sub>2</sub> engineered nanoparticles modulates gut inflammatory response and microbiota in mice. *Ecotoxicology and Environmental Safety*, 2022, 236, pp.113442. 10.1016/j.ecoenv.2022.113442 . hal-03627147

**HAL Id: hal-03627147**

**<https://hal.science/hal-03627147>**

Submitted on 22 Jul 2024

**HAL** is a multi-disciplinary open access archive for the deposit and dissemination of scientific research documents, whether they are published or not. The documents may come from teaching and research institutions in France or abroad, or from public or private research centers.

L'archive ouverte pluridisciplinaire **HAL**, est destinée au dépôt et à la diffusion de documents scientifiques de niveau recherche, publiés ou non, émanant des établissements d'enseignement et de recherche français ou étrangers, des laboratoires publics ou privés.



Distributed under a Creative Commons Attribution - NonCommercial 4.0 International License

Revised manuscript 03/03/2022

1

2 **Title page**

3 **Title**

4 Exposure to atmospheric Ag, TiO<sub>2</sub>, Ti and SiO<sub>2</sub> engineered nanoparticles modulates gut  
5 inflammatory response and microbiota in mice

6 **Author names and affiliations**

7 Eva Guilloteau<sup>1</sup>, Madjid Djouina<sup>1</sup>, Ségolène Caboche<sup>2</sup>, Christophe Waxin<sup>1</sup>, Karine Deboudt<sup>3</sup>,  
8 Delphine Beury<sup>2</sup>, David Hot<sup>2</sup>, Muriel Pichavant<sup>5</sup>, Laurent Dubuquoy<sup>1</sup>, David Launay<sup>1</sup>, Cécile  
9 Vignal<sup>1</sup>, Marie Choël<sup>4</sup>, Mathilde Body-Malapel<sup>1</sup>

10 1. Univ. Lille, Inserm, CHU Lille, U1286- INFINITE - Institute for Translational Research in  
11 Inflammation, F-59000, Lille, France

12 2. Univ. Lille, CNRS, Inserm, CHU Lille, Institut Pasteur de Lille, UMR2014 - US41 - PLBS-  
13 Plateformes Lilloises de Biologie & Santé, F-59000, Lille, France

14 3. Univ. Littoral Côte d'Opale, EA 4493 – LPCA - Laboratoire de Physico-Chimie de  
15 l'Atmosphère, 59140, Dunkerque, France

16 4. Univ. Lille, CNRS, UMR 8516 - LASIRE - Laboratoire de Spectroscopie pour les  
17 Interactions, la Réactivité et l'Environnement, F-59000, Lille, France

18 5. Univ. Lille, CNRS, Inserm, CHU Lille, Institut Pasteur de Lille, U1019 - UMR 9017 - CIIL  
19 - Center for Infection and Immunity of Lille, F-59000, Lille, France

20 **Corresponding author**

21 Mathilde BODY-MALAPEL, PhD

22 E-mail address:

23 mathilde.body@univ-lille.fr

24 Full postal address: Institute for Translational Research in Inflammation

25 Infinite - Univ. Lille, Inserm, CHU Lille, U1286

26 Faculté de Médecine - Pôle Recherche, 4ème étage Centre, Place Verdun, F-59045, Lille, Cedex

27 **Abstract**

28 The development of nanotechnologies is leading to greater abundance of engineered  
29 nanoparticles (EN) in the environment, including in the atmospheric air. To date, it has been  
30 shown that the most prevalent EN found in the air are silver (Ag), titanium dioxide (TiO<sub>2</sub>),  
31 titanium (Ti), and silicon dioxide (SiO<sub>2</sub>). As the intestinal tract is increasingly recognized as a  
32 target for adverse effects induced by inhalation of air particles, the aim of this study was to  
33 assess the impact of these 4 atmospheric EN on intestinal inflammation and microbiota. We  
34 assessed the combined toxicity effects of Ag, Ti, TiO<sub>2</sub>, and SiO<sub>2</sub> following a 28-day inhalation  
35 protocol in male and female mice. In distal and proximal colon, and in jejunum, EN mixture  
36 inhalation did not induce overt histological damage, but led to a significant modulation of  
37 inflammatory cytokine transcript abundance, including downregulation of *Tnfα*, *Ifnγ*, *Il1β*,  
38 *Il17a*, *Il22*, *Il10*, and *Cxcl1* mRNA levels in male jejunum. A dysbiosis was observed in cecal  
39 microbiota of male and female mice exposed to the EN mixture, characterized by sex-dependent  
40 modulations of specific bacterial taxa, as well as sex-independent decreased abundance of the  
41 Eggerthellaceae family. Under dextran sodium sulfate-induced inflammatory conditions,  
42 exposure to the EN mixture increased the development of colitis in both male and female mice.  
43 Moreover, the direct dose-response effects of individual and mixed EN on gut organoids was  
44 studied and Ag, TiO<sub>2</sub>, Ti, SiO<sub>2</sub>, and EN mixture were found to generate specific inflammatory  
45 responses in the intestinal epithelium. These results indicate that the 4 most prevalent  
46 atmospheric EN could have the ability to disturb intestinal homeostasis through direct  
47 modulation of cytokine expression in gut epithelium, and by altering the inflammatory response  
48 and microbiota composition following inhalation.

49

50 **Keywords:** Engineered Nanoparticles. Inhalation. Inflammation. Colitis. Organoid. Mixture.  
51 Microbiome. Digestive tract. Intestine.

52

## 53 **1. Introduction**

54

55 The International Organization for Standardization defines a nanoparticle as a nanomaterial  
56 with all three dimensions in the nanoscale, which is approximately 1 to 100 nm (Boverhof et  
57 al., 2013). Nanoparticles that are synthesized artificially for commercial use are called  
58 engineered nanoparticles (EN) (Prajitha et al., 2019). EN are prepared deliberately at the  
59 nanoscale because they exhibit properties that provide technological advantages compared with  
60 the bulk form of the same material (The Royal Society and The Royal Academy of Engineering,  
61 2004). Engineered nanoparticles usage is widespread, covering the energy sector,  
62 telecommunications industry, computing, agrichemicals (nanopesticides and nanofertilizers),  
63 and personal care products (Hansen et al., 2016). Nanotechnologies have also provided new  
64 opportunities in medicine mainly through the use of EN for diagnostic and therapeutic purposes  
65 (biomedical imaging, drug delivery, and targeting) (Rudramurthy and Swamy, 2018).  
66 Nanotechnology has become a key component in the modern world and the global  
67 nanotechnology market is expected to exceed USD \$125 billion by 2024 (Inshakova et al.,  
68 2020). In everyday life, humans are exposed to thousands of nanoparticles via dermal contact,  
69 inhalation, and ingestion (including parenteral administration) (Malakar et al., 2021). Although  
70 advances in the field of nanotechnology have resulted in a myriad of possibilities for  
71 technological improvement, the introduction of a wide range of novel EN to the environment  
72 and to humans, either by design or inadvertently, raises the possibility of harmful and/or  
73 unforeseen adverse effects. Indeed, inhalable nanoparticles can be transported in blood and the  
74 lymphatic system and bypass barriers within the body which are generally impermeable to

75 larger particles (Bakand et al., 2012). Especially noteworthy, studies have highlighted that  
76 ambient particulate matter (PM) exerts a deleterious impact on the intestinal tract of mice.  
77 Ambient ultrafine PM is similar in size to EN, but it is derived from natural and combustion  
78 processes. It has been shown in mice that inhalation of ambient ultrafine PM shortened villus  
79 length and infiltrated macrophages and neutrophils in the small intestine (Li et al., 2015).  
80 Moreover, another study in mice showed that ambient ultrafine PM inhalation led to epithelial  
81 injury with inflammatory cell infiltration and mucus depletion in the colon (X. Li et al., 2019).  
82 Regarding EN, toxicological studies have highlighted organ-specific toxicity of various  
83 nanoparticles following inhalation (Murugadoss et al., 2017; Kim et al., 2018; Hadrup et al.,  
84 2020; Sutunkova et al., 2020), but the impact of EN inhalation on the intestine has never been  
85 explored.

86 In this study, we focused on the most abundant EN found in air. Despite the general lack of  
87 qualitative and quantitative data on human exposure to EN, Hansen et al. (2016) have  
88 established “The Nanodatabase” (<http://www.nanodb.dk>), which is an online inventory of  
89 products claimed by manufacturers to contain nanomaterials or include nanotechnology. This  
90 database indicates that for inhalation, silver (Ag) is the most prevalent nanomaterial followed  
91 by titanium (Ti), titanium dioxide (TiO<sub>2</sub>), and silicon dioxide (SiO<sub>2</sub>) (Hansen et al., 2016). Ag  
92 and Ti nanoparticles are known for their biological and biomedical properties (Pereira et al.,  
93 2018). Both are often present in consumer products such as cosmetics, food additives, kitchen  
94 utensils, and toys. Ag nanoparticles exhibit antimicrobial activity and are used in the areas of  
95 food preservation, personal care products (shampoos, lotions, and toothpaste), spray  
96 disinfectants, antibacterial surfaces and textiles, nanomedicine, and dentistry (Lee and Jun,  
97 2019; Rogers et al., 2018; Tang and Zheng, 2018; Yin et al., 2020). Ti is utilized within artificial  
98 implants in dental and orthopaedic surgery (Chourifa et al., 2019). SiO<sub>2</sub> (including synthetic  
99 amorphous silica, or SAS) and TiO<sub>2</sub> are produced in high volumes and applied in many

100 consumer and food products. SiO<sub>2</sub> nanoparticles are used as food additive (E551) to prevent  
101 poor flow or caking particularly in powdered products. TiO<sub>2</sub> nanoparticles are extensively used  
102 as a pigment, a thickener, and an ultraviolet absorber in cosmetic and skin care products. TiO<sub>2</sub>  
103 allows osseointegration of artificial medical implants and bone (Gupta and Xie, 2018). In  
104 addition, TiO<sub>2</sub> and SiO<sub>2</sub> are used in protective coatings and for environmental treatment to  
105 protect products against environmental damage or in household water and air treatment. Both  
106 of these substances have been found in human tissues including jejunum and ileum (Peters et  
107 al., 2020). The aim of this study was to determine if the presence of these 4 EN in ambient air  
108 can result in intestinal adverse health effects. For this purpose, mice were exposed by inhalation  
109 to a mixture of Ag, Ti, TiO<sub>2</sub>, and SiO<sub>2</sub> nanoparticles, and the impact on intestinal tissues was  
110 analysed at steady-state and in the context of dextran sulfate sodium (DSS)-induced colitis, a  
111 model commonly used to mimic acute intestinal inflammation in mice. Moreover, the effects  
112 of individual Ag, Ti, TiO<sub>2</sub>, and SiO<sub>2</sub> EN were studied in intestinal organoids, the most advanced  
113 *in vitro* model for gut epithelium characterization.

114

## 115 **2. Materials and methods**

116

### 117 **2.1. Characterization of EN by transmission electron microscopy (TEM)**

118 SiO<sub>2</sub> in water (average particle size (APS) 20 nm), TiO<sub>2</sub> (anatase; APS 5-30 nm) in water, Ti  
119 powder (APS 60-80 nm), and Ag powder (APS 50-60 nm) were purchased from IoLiTec  
120 Nanomaterials. For physicochemical characterization, each nanoparticle sample was diluted in  
121 ultrapure water and deposited on TEM grids (Copper 200 mesh grids with carbon film, Agar  
122 Scientific<sup>TM</sup>). Once dried, each sample was observed by scanning electron microscopy (FEG-  
123 SEM), using a JEOL<sup>TM</sup> JSM7100F electron microscope equipped with a transmitted electron  
124 detector and 3 X-ray energy dispersive spectrometers (Bruker<sup>TM</sup> XFlash 6/30), enabling the

125 analysis of elements with atomic numbers greater than boron ( $Z \geq 5$ ). The microscope was  
126 operated at 15 kV with a probe current of 300 pA and a working distance suitable for X-ray  
127 detection (10 mm). All nanoparticle suspensions were used within 1 h after sonication.

128

## 129 **2.2. Animals and experimental design**

130 The animal protocol was approved by the regional bioethics committee (committee no.75;  
131 authorization no. CEEA 2016072517274040) and the animals received human care in  
132 accordance with the Guide for the Care and the Use of Laboratory Animals (National Research  
133 Council (US) Committee, 2011). Male and female C57BL/6JRj mice (aged 7 weeks) were  
134 purchased from Janvier Labs and housed under standard conventional conditions (Suppl. Fig.  
135 1A). The room relative humidity was 55% and the temperature was 21°C. Mice were randomly  
136 divided into the different exposure groups (n=10/group). Mice were placed 4 h/day, 5  
137 days/week for 28 days in a ventilated whole-body inhalation chamber that allowed free  
138 movement (inExpose, SCIREQ Scientific®). Nebulization was achieved using an Aeroneb  
139 Lab™ ultrasonic nebulizer (SCIREQ Scientific®) directly connected to a 5 L chamber and  
140 controlled through flexiWare software v.6 (SCIREQ Scientific®) according to the following  
141 parameters: bias flow of 2 L/min and nebulization rate of 0.083 ml/min, which we measured  
142 and controlled throughout the experiment. These parameters allowed the nebulization of the EN  
143 mixture at a concentration of 1 mg/m<sup>3</sup> in the chamber. Mice were euthanized the morning  
144 following the final exposure day. The distal colon, proximal colon, and jejunum were collected  
145 and stored for subsequent analyses.

146

## 147 **2.3. Gut histological analysis**

148 Formaldehyde-fixed intestinal tissues were embedded in paraffin, serially sectioned (4 µm),  
149 and stained with May-Grünwald and Giemsa (MGG). An inflammatory infiltration score was

150 blindly determined according to Li et al. (X. Li et al., 2019). This score is the sum of the  
151 infiltration score plus the percent area involved of each section. Infiltration was scored on a  
152 scale of 0 to 3 (0, no inflammatory cells; 1, infiltration around crypt bases; 2, infiltration of  
153 muscularis mucosa; 3, infiltration of submucosa), and the percent area of each section was  
154 scored on a scale of 0 to 4 (0, no involvement; 1,  $\leq 25\%$ ; 2,  $\leq 50\%$ ; 3,  $\leq 75\%$ ; 4,  $\leq 100\%$ ). Scoring  
155 was performed on distal colon, proximal colon, and jejunum (magnification 20X; 3 to 7 fields  
156 per section; 4 to 6 mice per group).

157

#### 158 **2.4. Quantification of transcriptional levels of cytokines and oxidative stress markers by** 159 **real-time PCR**

160 Total mRNA from intestinal tissues and organoids was extracted using a Nucleospin RNA II  
161 kit (Macherey-Nagel) according to manufacturer protocol. Reverse transcription was performed  
162 using a High Capacity cDNA Archive Kit and quantitative polymerase chain reaction (qPCR)  
163 with SYBR Green (Thermo Fisher Scientific). The primer sequences were designed using  
164 Primer Express 3 (Thermo Fisher Scientific) and are available upon request. Melting curve  
165 analyses were performed for each sample and gene to confirm the specificity of the  
166 amplification. Because exposure to EN mixture (ENM) did not cause any significant alterations  
167 in *Polr2a* mRNA expression, the relative expression of each gene of interest was normalized to  
168 the relative expression of this gene. The quantification of the target gene expression was based  
169 on the comparative cycle threshold (Ct) value. The fold changes in the target genes were  
170 analysed by the  $2^{-\Delta\Delta Ct}$  method.

171

#### 172 **2.5. Bacterial DNA extraction and Illumina MiSeq sequencing**

173 Genomic DNA was extracted from cecal content using the DNA Stool kit (Macherey-Nagel)  
174 according to manufacturer protocol. The quantity and the purity of DNA (expressed as the ratio

175 of absorbance at 260 nm and 280 nm (A260/A280)) were assessed using a NanoDrop®  
176 spectrophotometer (Ozyme). The sequencing library was generated by amplifying the V3-V4  
177 region of the bacterial 16S-rRNA gene using 16S rRNA amplicon generation for MiSeq with  
178 the primers Bact-0341 (5'-CCTACGGGNGGCWGCAG-3') and Bact-0785 (5'-  
179 GACTACHVGGGTATCTAATCC-3'). Individual samples were barcoded, pooled to construct  
180 the sequencing library, and sequenced using an Illumina MiSeq system to generate paired-end  
181 2x300 bp reads.

182

## 183 **2.6. Analysis of sequencing data**

184 Bioinformatic analyses were performed using the QIIME 2 pipeline (v.2020.2) (Bolyen et al.,  
185 2019). The Divisive Amplicon Denoising Algorithm 2 (DADA2) plug-in in QIIME2 was used  
186 to filter, dereplicate, identify chimeric sequences, and merge paired-end reads to obtain the set  
187 of amplicon sequence variants (ASVs) for each sample (Callahan et al., 2016). Then the  
188 representative sequences were picked for each ASV. The classify-sklearn plug-in in QIIME2,  
189 with the SILVA database (v.132) was applied to assign a taxonomic annotation to each  
190 representative ASV sequence. In the next step, ASVs identified as eukaryotic contamination  
191 (no contamination) and external contamination, identified with the decontam package (15 ASV;  
192 1599 reads), were filtered out (Davis et al., 2018). Diversity metrics ( $\alpha$  and  $\beta$ ) were obtained  
193 with the QIIME2 core-metrics-phylogenetic plug-in, with p-sampling depth parameter fixed to  
194 11916 reads which corresponded to the total frequency that each sample should be rarefied to  
195 before computing diversity metrics. This sampling depth allowed retention of >59% of reads  
196 discarding no sample.

197

## 198 **2.7. Dextran sodium sulfate (DSS)-induced colitis**

199 Colitis was induced by adding 2% (w/v) DSS (TdB Labs) in the drinking water for 6 days.  
200 Fresh DSS solutions were prepared every 2 days. Mice body weight was recorded during the  
201 experiment. At necropsy, colon was carefully dissected and its weight and size were measured.  
202 Colon was then either immediately frozen or fixed in 4% formaldehyde (VWR Chemicals).

203

## 204 **2.8. Organoid study**

205 Murine organoids were derived from colon tissue of male C57BL/6 mice (aged 7 weeks). As  
206 described in Co et al. (2019), tissue fragments were incubated in 2 mM EDTA in cold chelation  
207 buffer on ice for 30 minutes (Co et al., 2019). The EDTA buffer was removed and tissue  
208 fragments were vigorously shaken in cold chelation buffer to isolate intestinal crypts. Isolated  
209 crypts were embedded in Matrigel (Growth Factor Reduced; Corning) on ice and seeded into a  
210 24-well tissue culture plate. Then 500  $\mu$ L of growth media and 50% L-WRN-conditioned media  
211 were added. Colon organoids were grown embedded in Matrigel for 7-14 days with growth  
212 media. Matrigel-embedded organoids were solubilized in 5 mM EDTA in PBS for 1 h at 4°C  
213 on a rotating platform. Organoids were centrifuged at 200 x g for 3 min at 4°C and the  
214 supernatant was removed. The pellet was resuspended in growth media in ultra-low attachment  
215 24-well tissue culture plates (Corning Costar). Suspended organoids were incubated at 37°C  
216 with 5% CO<sub>2</sub> for 2 days so that they could invert and present the apical side to the exterior.  
217 Inverted organoids were treated with 0.02, 0.2, and 2  $\mu$ M of Ag, SiO<sub>2</sub>, Ti, and TiO<sub>2</sub> EN for 24  
218 h. Cell death was measured using the Cytotoxicity Detection Kit (LDH) (Roche) according to  
219 the manufacturer's protocol.

220

## 221 **2.9. Statistical analysis**

222 Results are expressed as mean  $\pm$  SEM. Normality tests were performed for each parameter using  
223 the D'agostino-Pearson normality test. Since the data was not normally distributed, the

224 statistical significance of differences between experimental groups was calculated using the  
225 Mann-Whitney U test (GraphPad, San Diego, CA).

226

### 227 **3. Results**

228

#### 229 **3.1. Characterization of EN**

230 Figure 1A shows typical TEM images and EDX spectra of the 4 EN samples. Image analysis  
231 of 308 Ag particles indicated an area equivalent mean diameter of 8.6 nm ( $SD=2.4$  nm). Image  
232 analysis of 261 SiO<sub>2</sub> particles yielded a mean equivalent diameter of 21.1 nm ( $SD=6.0$  nm). In  
233 the case of Ti samples, we noticed the presence of aggregated spherical Ti nanoparticles with  
234 individual particle sizes ranging from 5 nm to 350 nm. Despite several attempts to deposit a  
235 uniform layer of TiO<sub>2</sub> particles, the noisy TEM image did not allow for statistical size analysis  
236 but an average equivalent diameter of 14.6 nm was estimated by manual sizing. X-ray spectra  
237 did not show the presence of contaminant elements. The copper peak was attributed to the TEM  
238 copper mesh support grid. As shown in the elemental map of the ENM (Fig. 1B), all expected  
239 elements (Si, Ag, Ti, and O) were identified by X-ray emission spectrometry. Chemical and  
240 topographic maps of the ENM showed spherical particles containing titanium (Ti or TiO<sub>2</sub>)  
241 covered with Ag and SiO<sub>2</sub> nanoparticles.

242

#### 243 **3.2. Effects of ENM exposure on gut inflammation**

244 Adult male and female mice were exposed by inhalation to the ENM or to control inhalation  
245 (Suppl. Fig. 1A). Body weight over the 28-day duration of the experiment did not vary  
246 significantly in males or females ( $p=0.7$  for males,  $p=0.4$  for females, Suppl. Fig. 1B). To assess  
247 the inflammatory status of intestinal tissues, we performed a histological scoring of  
248 inflammation in distal colon, proximal colon, and jejunum. In males, the inflammatory

249 infiltration score did not change between the groups ( $p=0.8$  for distal colon,  $p=0.4$  for proximal  
250 colon, Fig. 2A-C), even if a trend to enhancement of this score was observed in jejunum ( $p=0.1$ ).  
251 For comparison of cytokines, in distal colon, transcript levels of *Tnf $\alpha$* , *Ifn $\gamma$* , *Il22*, and *IL10* were  
252 significantly increased in ENM-exposed mice compared to control mice ( $p=0.007$ ,  $0.0002$ ,  $0.01$   
253 and  $0.03$  respectively, Fig. 2D). In proximal colon, there was a significant enhancement of the  
254 mRNA levels of *Tnf $\alpha$* , *Il1 $\beta$* , *Il10*, and *Cxcl1* ( $p=0.04$ ,  $0.007$ ,  $0.001$  and  $0.03$  respectively, Fig.  
255 2E). In jejunum, ENM exposure led to a drastic decrease of *Tnf $\alpha$* , *Ifn $\gamma$* , *Il1 $\beta$* , *Il17a*, *Il22*, *IL10*,  
256 and *Cxcl1* mRNA expression ( $p=0.04$ ,  $0.004$ ,  $0.001$ ,  $0.004$ ,  $<0.0001$ ,  $<0.0001$ ,  $0.002$   
257 respectively, Fig. 2F).

258 In female mice, exposure to ENM did not induce significant variation of inflammatory  
259 infiltration score in distal colon, proximal colon, and jejunum ( $p=0.4$  for distal colon and  
260 jejunum,  $p=0.6$  for proximal colon, Fig. 3A-C). *Cxcl1* transcripts were down-regulated in distal  
261 colon of ENM-exposed mice ( $p=0.01$ , Fig. 3D). A decrease of *Il1 $\beta$*  in proximal colon and a  
262 reduction of *Tnf $\alpha$* , *Il1 $\beta$*  and *Il22* in jejunum of ENM-exposed mice compared to control mice  
263 was also observed ( $p=0.005$ ,  $0.0002$ ,  $0.01$  and  $0.009$  respectively, Fig. 3E-F).

264

### 265 **3.3. Effects of ENM exposure on gut microbiota.**

266 The bacterial diversity in cecal content was determined by pyrosequencing of the bacterial 16S  
267 rRNA genes. Exposure to ENM did not significantly affect  $\alpha$ -diversity (data not shown). In  
268 males, unweighted uniFrac index showed a significant increase of  $\beta$ -diversity in ENM-exposed  
269 mice compared to control mice ( $p=0.004$ ; Fig. 4A). The relative abundance of ASVs at phylum,  
270 class, order, and family taxonomic levels was compared. The major phyla were Firmicutes and  
271 Bacteroidetes and the Tenericutes were less abundant in ENM-exposed mice (Fig. 4B). ENM  
272 exposure also induced in male mice a decrease of Coriobacteriia and Mollicutes classes, and of  
273 Coriobacteriales and Mollicutes RF39 orders (Fig. 4C-D). The only family which showed

274 significantly different abundance in exposed male mice was Eggerthellaceae (Fig. 4E). In  
275 females, the unweighted uniFrac index was increased significantly after exposure to ENM  
276 ( $p=0.008$ ; Suppl. Fig. 2). As expected, in females, the cecum microbiota was also mostly  
277 composed of bacteria belonging to Firmicutes and Bacteroidetes phyla (Fig. 5A). The relative  
278 abundance of Proteobacteria and Actinobacteria was decreased in ENM-exposed mice. At the  
279 class level, abundances of Deltaproteobacteria and Coriobacteriia were lower after exposure to  
280 ENM (Fig. 5B). A significant reduction of the levels of Desulfovibrionales and Coriobacteriales  
281 orders in ENM-exposed female mice was also observed (Fig. 5C). Finally, like males, females  
282 showed a lower abundance of Eggerthellaceae family after exposure to ENM (Fig. 5D).

283

### 284 **3.4. Effects of ENM exposure in a mouse model of colitis**

285 Male mice were submitted to DSS administration in the last 6 days of the ENM inhalation  
286 protocol (Suppl Fig. 3A). A significant body weight loss was observed in ENM-exposed mice  
287 compared to control mice from the third to the last day of DSS treatment ( $p=0.004$  at day 6,  
288 Fig. 6A). The colon weight/size ratio and the histological inflammatory infiltration score were  
289 not modified between the 2 groups of mice ( $p=0.2$  and  $0.08$  respectively, Fig. 6B and Suppl  
290 Fig. 3B). The transcript levels of *Tnf $\alpha$*  and *Ifn $\gamma$*  were higher in colitic ENM-exposed mice than  
291 in colitic control mice ( $p=0.002$  and  $0.01$  respectively, Fig. 6C).

292 The same protocol was performed with female mice (Suppl Fig. 3C). Colitic ENM-exposed  
293 mice lost more weight than colitic control mice from the fourth to the last day of DSS treatment  
294 ( $p<0.0001$  at day 6, Fig. 6D). The colon weight/size ratio was significantly increased in the  
295 ENM-exposed group, as well as the histological score of colitis ( $p=0.001$  and  $0.048$   
296 respectively, Fig. 6E and Suppl Fig. 3D). The expression of inflammatory cytokines was  
297 upregulated in the colon of ENM-exposed mice, particularly *Ifn $\gamma$*  and *Cxcl1* ( $p=0.004$  and  
298  $0.0003$  respectively, Fig. 6F). These data show that ENM exposure induces higher susceptibility

299 to colitis development, and that this increased sensitivity to colitis is greater in females than in  
300 males.

301

### 302 **3.5. Effects of EN on gut organoids**

303 Then the effects of individual EN and ENM on intestinal epithelium were assessed. For this  
304 purpose, mouse intestinal organoids which model *in vitro* a 3D microarchitecture and possess  
305 a cellular composition resembling native intestinal epithelium were used. The organoids were  
306 generated from pluripotent stem cells which were differentiated into enterocytes, stem cells,  
307 goblet cells, Paneth cells, enteroendocrine cells, and mesenchymal cells. Organoids were  
308 treated with 0.02, 0.2, and 2  $\mu\text{M}$  of Ag, SiO<sub>2</sub>, Ti, TiO<sub>2</sub> EN and ENM for 24 h. These  
309 concentrations did not induce cytotoxicity as confirmed by the LDH assay (Suppl. Fig. 3). Ag  
310 enhanced the expression of the chemokines *Ccl5*, *Ccl20*, and *Ccl10* and of the alarmins *Il1 $\alpha$*   
311 and *Il33* ( $p=0.03$  for all genes at 0.2  $\mu\text{M}$ , Fig. 7A). SiO<sub>2</sub> increased the transcript levels of *Tnf $\alpha$*   
312 and *Cxcl10* even at the lowest dosage, and enhanced *Il1 $\alpha$*  expression ( $p=0.03$  for all genes at 2  
313  $\mu\text{M}$ , Fig. 7B). Ti increased *Tnf $\alpha$* , *Ccl5*, *Cxcl10*, and *Il33* and decreased *Cxcl1* mRNA levels  
314 ( $p=0.03$  for all genes at 0.2  $\mu\text{M}$ , Fig. 7C). TiO<sub>2</sub> downregulated and upregulated the expression  
315 of *Cxcl1* and *Il33*, respectively ( $p=0.03$  for both genes at 0.2  $\mu\text{M}$ , Fig. 7D). The mixture of the  
316 4 EN induced significant variations mainly at 2 $\mu\text{M}$  (Fig.7E). It totally annihilated the *CCl5* and  
317 *Il1 $\alpha$*  mRNA expression, which became undetermined. It increased the transcript levels of  
318 *CCl20*, *Cxcl1* and *Il33* ( $p=0.03$  for all genes at 0.2 $\mu\text{M}$ ).

319

## 320 **4. Discussion**

321 The fate of inhaled nanoparticles has been studied in lung, brain, and at the systemic level, but  
322 little is known about responses in the digestive tract (Aalapati et al., 2014; Cupaioli et al., 2014;  
323 Miller et al., 2017). However, it has been shown that inhaled particles can be directed to the

324 intestinal tract via the mucociliary clearance process (Smith et al., 2002). This process mainly  
325 affects larger particles, but also includes nanoparticles. For example, detection of TiO<sub>2</sub>  
326 nanoparticles in feces following inhalation demonstrated a mucociliary clearance and ingestion  
327 of nanoparticles (Pujalté et al., 2017). Moreover, inhaled Ag nanoparticles are cleared via the  
328 larynx into the gastro-intestinal tract, and in addition, via blood, liver, and gall bladder into the  
329 gastro-intestinal tract with one common excretional pathway: via feces out of the body  
330 (Kreyling et al., 2020). Nanoparticles can translocate into the bloodstream from which they can  
331 then impact all tissues of the body, either by direct contact or by various indirect routes (Miller  
332 et al., 2017). The constant increase in EN production worldwide has led to the presence of Ag,  
333 SiO<sub>2</sub>, Ti, and TiO<sub>2</sub> nanoparticles in the air. In addition to potential high workplace exposures to  
334 each of these EN, chronic low-dose exposure of the general population may occur if current  
335 production trends continue. It is therefore important to assess the health effects of such  
336 exposures, and particularly on the intestinal tissues which are increasingly recognized as an  
337 important target for inhaled particles (Feng et al., 2020; Vignal et al., 2021). In this study,  
338 healthy adult mice were exposed for 4 h per day for 28 days to a mixture of the 4 EN most  
339 commonly found in ambient air, each at a dose of 1 mg/m<sup>3</sup>. The range of EN present in the air  
340 is not known, so it is not currently possible to assess the relevance of this dose to human  
341 exposure. However, this dosage is within the range that has been used in other similar studies.  
342 For example, Umezawa et al. (2018) exposed mice in an inhalation chamber to 4.6 or 37 mg/m<sup>3</sup>  
343 of Printex 90 carbon black nanoparticles for 15 days (Umezawa et al., 2018). Wahle et al. (2020)  
344 exposed mice via nose only inhalation to CeO<sub>2</sub> nanoparticles with varying amounts of Zr-  
345 doping (0%, 27%, or 78% Zr) over a 4-week period (4 mg/m<sup>3</sup> for 3 h/day, 5 days/week) (Wahle  
346 et al., 2020). These experimental protocols allow a primary toxicological evaluation ahead of  
347 more in-depth dose-response studies.

348 At the histological level, we did not observe any significant differences between exposed and  
349 control mice, showing that inhalation of ENM did not induce drastic damage in intestinal  
350 tissues. However, more sensitive methods such as qPCR allowed us to highlight sex-specific  
351 modifications. In males, we observed upregulation of numerous inflammatory cytokines in both  
352 distal and proximal colon. By contrast, in male jejunum, all the inflammatory markers were  
353 found strongly downregulated in mice exposed to ENM. In females, the pattern of inflammatory  
354 biomarkers was only slightly modified in distal and proximal colon. Moreover, inhalation of  
355 ENM induced a drastic decrease in expression of several inflammatory cytokines in jejunum,  
356 similarly to males. Thus, under basal conditions, inhalation of ENM did not induce overt  
357 inflammation in intestinal tissue. However, among the few inflammatory markers quantified,  
358 several were found to be significantly modified in favor of micro-inflammation, particularly in  
359 male colon. In accordance with these data, a micro-inflammatory state has been described after  
360 oral exposure to TiO<sub>2</sub>, SiO<sub>2</sub>, and Ag nanoparticles (Lamas et al., 2020).

361 Modifications of cecal microbiota composition were compared between exposed and non-  
362 exposed mice at several taxonomic levels. Males exposed to ENM showed a decreased  
363 abundance of the Tenericutes phylum, Mollicutes class, and Mollicutes RF39 order. In mice,  
364 Mollicutes have been shown to be decreased in TNBS-induced colitis (P. Li et al., 2019) and  
365 after subchronic oral toxic metal exposure (Zhai et al., 2017). The abundance of *Mollicutes* is  
366 decreased in fecal microbiota of patients with colon Crohn's disease and ulcerative colitis, and  
367 shown to be increased in a patient with ileal Crohn's disease (Willing et al., 2010). Gut  
368 microbiota of obese patients also shows a greater proportion of Mollicutes (Crovesy et al.,  
369 2020). Moreover, we observed a reduction of Proteobacteria phylum, Deltaproteobacteria class,  
370 and Desulfovibrionales order in females exposed to ENM. The presence of Desulfovibrionales  
371 bacteria in gut microbiota has been associated with Parkinson's disease (Murros et al., 2021)  
372 and autism spectrum disorder (de Theije et al., 2014). A 16S microbiota sequencing study has

373 also shown that bacteria of the Desulfovibrionales order were present within the ileal  
374 submucosal tissues of most Crohn's disease patients but absent in the control group (Chiodini  
375 et al., 2015). Notably, we identified microbiota modifications by ENM exposure which were  
376 common to both males and females. Microbiota of ENM-exposed males was characterized by  
377 less abundance of Coriobacteriia class, Coriobacteriales order, and Eggerthellaceae family.  
378 Similarly, microbiota of ENM-exposed females exhibited lower levels of Actinobacteria  
379 phylum, Coriobacteriia class, Coriobacteriales order, and Eggerthellaceae family. The  
380 abundance of Eggerthellaceae has been associated with the intensity of 5-fluorouracil-induced  
381 intestinal mucositis in mice (Chen et al., 2021). It was found to be increased in gut of patients  
382 with psoriasis (Sikora et al., 2020). Furthermore, this family has been suggested to play a critical  
383 role in occurrence and development of osteoporosis (Wen et al., 2020). Taken together, these  
384 results show that ENM exposure induced sex-dependent and -independent modifications of  
385 fecal microbiota composition, which could play a role in the micro-inflammatory state observed  
386 in mouse gut.

387 The sex-dependency of EN toxicity has been widely observed (Bao et al., 2020; Lovaković et  
388 al., 2021; Ma et al., 2018). This variability between males and females is often attributed to the  
389 differences in sexual hormone signalling. Androgens, estrogens, and progesterone modulate  
390 intestinal inflammation and shape gut microbiota (Pace and Watnick, 2021). Beyond the  
391 differences in the expression of sex hormones, a sexual dimorphism in peripheral and intestinal  
392 immunity, as well as in intestinal microbiome is known (Elderman et al., 2018). The tissue  
393 accumulation and clearance of nanoparticles can be also sex-specific (Bao et al., 2020; Lee et  
394 al., 2020). In *ex vivo* ileal tissue, a sex-dependency has been demonstrated for cytokines,  
395 chemokines and intestinal permeability genes in response to Ag EN (Gokulan et al., 2021).  
396 Finally, the sex-dependency of EN toxicity can be explained by sex specific differences of EN

397 uptake at the cellular level, as demonstrated in amniotic stem cells and in primary fibroblasts  
398 (Serpooshan et al., 2018).

399 Under inflammatory conditions, both male and female mice exposed to ENM had a greater  
400 susceptibility to DSS-induced colitis. Therefore, despite low deleterious effects in healthy  
401 individuals, inhalation of ENM caused visible clinical effects in susceptible individuals. These  
402 data suggest that inhalation of ENM could aggravate diseases mediated by the immune system  
403 such as inflammatory bowel diseases.

404 We also investigated the potential of each EN to disturb the inflammatory response in intestinal  
405 epithelium. Both Ti and TiO<sub>2</sub> decreased expression of *Cxcl1* and increased expression of *Il33*.  
406 Ag and Ti had a strong ability to enhance the expression *Cxcl10* (10- and 19-fold, respectively,  
407 at 0.2 μM). Overall, TiO<sub>2</sub> had the least impact on intestinal inflammatory response, whereas it  
408 is the EN with the most documented deleterious effects on intestinal health (Rinninella et al.,  
409 2021). Accordingly, Kämpfer et al. observed stronger toxic effects of polyvinylpyrrolidone-  
410 capped Ag engineered nanomaterials than TiO<sub>2</sub> in Caco-2 and HT-29-MTX-E12 monocultures  
411 (Kämpfer et al., 2021). *Ex vivo*, treatment with 20 μg/mL of Ag EN induced sex-dependent  
412 alterations of cytokine secretion in human excised intestinal tissues (Gokulan et al., 2021). The  
413 mixture of the 4 EN induced a paradoxical response, by enhancing the expression of certain  
414 cytokines (16-fold increase of *Il33* levels), and by very strongly reducing the expression of  
415 other cytokines: the expression of *CCl5* and of *Il1α* were completely shunted, this latter type of  
416 modification was not observed following exposure to EN individually. As a whole, each of the  
417 4 tested EN as well as ENM elicited specific responses in colonoids.

## 418 **Conclusion**

419 The presence of EN in the air breathed by mice caused sex-dependent intestinal disturbances  
420 regarding inflammatory status and microbiota composition. Likewise, inhalation of ENM

421 increased susceptibility to DSS-induced colitis in mice. We also showed that exposure to Ag,  
422 SiO<sub>2</sub>, Ti, and TiO<sub>2</sub> EN led to specific inflammatory responses in gut epithelium. These findings  
423 suggest that respiratory exposure to common formulations of nanoscale particulates may  
424 facilitate the induction of a pro-inflammatory state localized within the intestine, alterations in  
425 gut microbiota composition, and modulation of susceptibility to chronic inflammatory  
426 conditions with the GI tract. Moreover, many of these effects may be differentially observed in  
427 exposed males and females, providing a new evidence of the sex-specificity of gut response to  
428 environmental chemicals.

429

### 430 **Funding**

431 This work was supported by the Hauts de France Region and the Ministère de l'Enseignement  
432 Supérieur et de la Recherche (CPER Climibio), and the European Fund for Regional Economic  
433 Development.

434

### 435 **Acknowledgements**

436 We thank Thomas Hubert and the staff of the animal facility of Lille for animal care. We thank  
437 Bernadette Leu for her broad-spectrum help. Editorial assistance, in the form of language  
438 editing and correction, was provided by XpertScientific Editing and Consulting Services.

439

### 440 **References**

- 441 Aalapati, S., Ganapathy, S., Manapuram, S., Anumolu, G., Prakya, B.M., 2014. Toxicity and  
442 bio-accumulation of inhaled cerium oxide nanoparticles in CD1 mice. *Nanotoxicology*  
443 8, 786–798. <https://doi.org/10.3109/17435390.2013.829877>  
444 Bakand, S., Hayes, A., Dechsakulthorn, F., 2012. Nanoparticles: A review of particle  
445 toxicology following inhalation exposure. *Inhal. Toxicol.* 24, 125–35.  
446 <https://doi.org/10.3109/08958378.2010.642021>  
447 Bolyen, E., Rideout, J.R., Dillon, M.R., Bokulich, N.A., Abnet, C.C., Al-Ghalith, G.A.,  
448 Alexander, H., Alm, E.J., Arumugam, M., Asnicar, F., Bai, Y., Bisanz, J.E., Bittinger,  
449 K., Brejnrod, A., Brislawn, C.J., Brown, C.T., Callahan, B.J., Caraballo-Rodríguez,  
450 A.M., Chase, J., Cope, E.K., Da Silva, R., Diener, C., Dorrestein, P.C., Douglas,

- 451 G.M., Durall, D.M., Duvall, C., Edwardson, C.F., Ernst, M., Estaki, M., Fouquier, J.,  
 452 Gauglitz, J.M., Gibbons, S.M., Gibson, D.L., Gonzalez, A., Gorlick, K., Guo, J.,  
 453 Hillmann, B., Holmes, S., Holste, H., Huttenhower, C., Huttley, G.A., Janssen, S.,  
 454 Jarmusch, A.K., Jiang, L., Kaehler, B.D., Kang, K.B., Keefe, C.R., Keim, P., Kelley,  
 455 S.T., Knights, D., Koester, I., Kosciulek, T., Kreps, J., Langille, M.G.I., Lee, J., Ley,  
 456 R., Liu, Y.-X., Lofthfield, E., Lozupone, C., Maher, M., Marotz, C., Martin, B.D.,  
 457 McDonald, D., McIver, L.J., Melnik, A.V., Metcalf, J.L., Morgan, S.C., Morton, J.T.,  
 458 Naimey, A.T., Navas-Molina, J.A., Nothias, L.F., Orchanian, S.B., Pearson, T.,  
 459 Peoples, S.L., Petras, D., Preuss, M.L., Pruesse, E., Rasmussen, L.B., Rivers, A.,  
 460 Robeson, M.S., Rosenthal, P., Segata, N., Shaffer, M., Shiffer, A., Sinha, R., Song,  
 461 S.J., Spear, J.R., Swafford, A.D., Thompson, L.R., Torres, P.J., Trinh, P., Tripathi, A.,  
 462 Turnbaugh, P.J., Ul-Hasan, S., van der Hooft, J.J.J., Vargas, F., Vázquez-Baeza, Y.,  
 463 Vogtmann, E., von Hippel, M., Walters, W., Wan, Y., Wang, M., Warren, J., Weber,  
 464 K.C., Williamson, C.H.D., Willis, A.D., Xu, Z.Z., Zaneveld, J.R., Zhang, Y., Zhu, Q.,  
 465 Knight, R., Caporaso, J.G., 2019. Reproducible, interactive, scalable and extensible  
 466 microbiome data science using QIIME 2. *Nat. Biotechnol.* 37, 852–857.  
 467 <https://doi.org/10.1038/s41587-019-0209-9>
- 468 Boverhof, D.R., Krieger, S.M., Hotchkiss, J.A., Stebbins, K.E., Thomas, J., Woolhiser, M.R.,  
 469 2013. Assessment of the immunotoxic potential of trichloroethylene and  
 470 perchloroethylene in rats following inhalation exposure. *J. Immunotoxicol.* 10, 311–  
 471 320. <https://doi.org/10.3109/1547691X.2012.735275>
- 472 Callahan, B.J., McMurdie, P.J., Rosen, M.J., Han, A.W., Johnson, A.J.A., Holmes, S.P., 2016.  
 473 DADA2: High-resolution sample inference from Illumina amplicon data. *Nat.*  
 474 *Methods* 13, 581–583. <https://doi.org/10.1038/nmeth.3869>
- 475 Chen, K.-J., Chen, Y.-L., Ueng, S.-H., Hwang, T.-L., Kuo, L.-M., Hsieh, P.-W., 2021.  
 476 Neutrophil elastase inhibitor (MPH-966) improves intestinal mucosal damage and gut  
 477 microbiota in a mouse model of 5-fluorouracil-induced intestinal mucositis. *Biomed.*  
 478 *Pharmacother.* 134, 111152. <https://doi.org/10.1016/j.biopha.2020.111152>
- 479 Chiodini, R.J., Dowd, S.E., Chamberlin, W.M., Galandiuk, S., Davis, B., Glassing, A., 2015.  
 480 Microbial Population Differentials between Mucosal and Submucosal Intestinal  
 481 Tissues in Advanced Crohn’s Disease of the Ileum. *PLOS ONE* 10, e0134382.  
 482 <https://doi.org/10.1371/journal.pone.0134382>
- 483 Chourifa, H., Bouloussa, H., Migonney, V., Falentin-Daudré, C., 2019. Review of titanium  
 484 surface modification techniques and coatings for antibacterial applications. *Acta*  
 485 *Biomater.* 83, 37–54. <https://doi.org/10.1016/j.actbio.2018.10.036>
- 486 Co, J.Y., Margalef-Català, M., Li, X., Mah, A.T., Kuo, C.J., Monack, D.M., Amieva, M.R.,  
 487 2019. Controlling Epithelial Polarity: A Human Enteroid Model for Host-Pathogen  
 488 Interactions. *Cell Rep.* 26, 2509-2520.e4. <https://doi.org/10.1016/j.celrep.2019.01.108>
- 489 Crovesy, L., Masterson, D., Rosado, E.L., 2020. Profile of the gut microbiota of adults with  
 490 obesity: a systematic review. *Eur. J. Clin. Nutr.* 74, 1251–1262.  
 491 <https://doi.org/10.1038/s41430-020-0607-6>
- 492 Cupaioli, F.A., Zucca, F.A., Boraschi, D., Zecca, L., 2014. Engineered nanoparticles. How  
 493 brain friendly is this new guest? *Prog. Neurobiol.* 119–120, 20–38.  
 494 <https://doi.org/10.1016/j.pneurobio.2014.05.002>
- 495 Davis, N.M., Proctor, D.M., Holmes, S.P., Relman, D.A., Callahan, B.J., 2018. Simple  
 496 statistical identification and removal of contaminant sequences in marker-gene and  
 497 metagenomics data. *Microbiome* 6, 226. <https://doi.org/10.1186/s40168-018-0605-2>
- 498 de Theije, C.G.M., Wopereis, H., Ramadan, M., van Eijndthoven, T., Lambert, J., Knol, J.,  
 499 Garssen, J., Kraneveld, A.D., Oozeer, R., 2014. Altered gut microbiota and activity in

- 500 a murine model of autism spectrum disorders. *Brain. Behav. Immun.* 37, 197–206.  
501 <https://doi.org/10.1016/j.bbi.2013.12.005>
- 502 Feng, J., Cavallero, S., Hsiai, T., Li, R., 2020. Impact of air pollution on intestinal redox  
503 lipidome and microbiome. *Free Radic. Biol. Med.*  
504 <https://doi.org/10.1016/j.freeradbiomed.2019.12.044>
- 505 Gokulan, K., Williams, K., Orr, S., Khare, S., 2021. Human Intestinal Tissue Explant  
506 Exposure to Silver Nanoparticles Reveals Sex Dependent Alterations in Inflammatory  
507 Responses and Epithelial Cell Permeability. *Int. J. Mol. Sci.* 22, 9.  
508 <https://doi.org/10.3390/ijms22010009>
- 509 Gupta, R., Xie, H., 2018. Nanoparticles in Daily Life: Applications, Toxicity and Regulations.  
510 *J. Environ. Pathol. Toxicol. Oncol.* 37.  
511 <https://doi.org/10.1615/JEnvironPatholToxicolOncol.2018026009>
- 512 Hadrup, N., Sharma, A.K., Loeschner, K., Jacobsen, N.R., 2020. Pulmonary toxicity of silver  
513 vapours, nanoparticles and fine dusts: A review. *Regul. Toxicol. Pharmacol.* RTP 115,  
514 104690. <https://doi.org/10.1016/j.yrtph.2020.104690>
- 515 Hansen, S.F., Heggelund, L.R., Besora, P.R., Mackevica, A., Boldrin, A., Baun, A., 2016.  
516 Nanoproducts—what is actually available to European consumers? *Environ. Sci. Nano*  
517 3, 169–180.
- 518 Inshakova, E., Inshakova, A., Goncharov, A., 2020. Engineered nanomaterials for energy  
519 sector: market trends, modern applications and future prospects. *IOP Conf. Ser. Mater.*  
520 *Sci. Eng.* 971, 032031. <https://doi.org/10.1088/1757-899X/971/3/032031>
- 521 Kämpfer, A.A.M., Busch, M., Büttner, V., Bredeck, G., Stahlmecke, B., Hellack, B., Masson,  
522 I., Sofranko, A., Albrecht, C., Schins, R.P.F., 2021. Model Complexity as  
523 Determining Factor for In Vitro Nanosafety Studies: Effects of Silver and Titanium  
524 Dioxide Nanomaterials in Intestinal Models. *Small* 17, 2004223.  
525 <https://doi.org/10.1002/sml.202004223>
- 526 Kim, Y.-S., Chung, Y.-H., Seo, D.-S., Choi, H.-S., Lim, C.-H., 2018. Twenty-Eight-Day  
527 Repeated Inhalation Toxicity Study of Aluminum Oxide Nanoparticles in Male  
528 Sprague-Dawley Rats. *Toxicol. Res.* 34, 343–354.  
529 <https://doi.org/10.5487/TR.2018.34.3.343>
- 530 Kreyling, W.G., Holzwarth, U., Hirn, S., Schleh, C., Wenk, A., Schäffler, M., Haberl, N.,  
531 Gibson, N., 2020. Quantitative biokinetics over a 28 day period of freshly generated,  
532 pristine, 20 nm silver nanoparticle aerosols in healthy adult rats after a single 1½-hour  
533 inhalation exposure. *Part. Fibre Toxicol.* 17, 21. <https://doi.org/10.1186/s12989-020-00347-1>
- 534
- 535 Lamas, B., Martins Breyner, N., Houdeau, E., 2020. Impacts of foodborne inorganic  
536 nanoparticles on the gut microbiota-immune axis: potential consequences for host  
537 health. *Part. Fibre Toxicol.* 17, 19. <https://doi.org/10.1186/s12989-020-00349-z>
- 538 Lee, S.H., Jun, B.-H., 2019. Silver Nanoparticles: Synthesis and Application for  
539 Nanomedicine. *Int. J. Mol. Sci.* 20. <https://doi.org/10.3390/ijms20040865>
- 540 Li, P., Lei, J., Hu, G., Chen, X., Liu, Z., Yang, J., 2019. Matrine mediates inflammatory  
541 response via gut microbiota in TNBS-induced murine colitis. *Front. Physiol.* 10, 28.
- 542 Li, R., Navab, K., Hough, G., Daher, N., Zhang, M., Mittelstein, D., Lee, K., Pakbin, P.,  
543 Saffari, A., Bhetraratana, M., Sulaiman, D., Beebe, T., Wu, L., Jen, N., Wine, E.,  
544 Tseng, C.-H., Araujo, J.A., Fogelman, A., Sioutas, C., Navab, M., Hsiai, T.K., 2015.  
545 Effect of exposure to atmospheric ultrafine particles on production of free fatty acids  
546 and lipid metabolites in the mouse small intestine. *Environ. Health Perspect.* 123, 34–  
547 41. <https://doi.org/10.1289/ehp.1307036>
- 548 Li, X., Sun, H., Li, B., Zhang, X., Cui, J., Yun, J., Yang, Y., Zhang, L., Meng, Q., Wu, S.,  
549 Duan, J., Yang, H., Wu, J., Sun, Z., Zou, Y., Chen, R., 2019. Probiotics Ameliorate

- 550 Colon Epithelial Injury Induced by Ambient Ultrafine Particles Exposure. *Adv. Sci.*  
551 *Weinh. Baden-Wurt. Ger.* 6, 1900972. <https://doi.org/10.1002/advs.201900972>
- 552 Malakar, A., Kanel, S.R., Ray, C., Snow, D.D., Nadagouda, M.N., 2021. Nanomaterials in the  
553 environment, human exposure pathway, and health effects: A review. *Sci. Total*  
554 *Environ.* 759, 143470. <https://doi.org/10.1016/j.scitotenv.2020.143470>
- 555 Miller, M.R., Raftis, J.B., Langrish, J.P., McLean, S.G., Samutrtai, P., Connell, S.P., Wilson,  
556 S., Vesey, A.T., Fokkens, P.H.B., Boere, A.J.F., Krystek, P., Campbell, C.J., Hadoke,  
557 P.W.F., Donaldson, K., Cassee, F.R., Newby, D.E., Duffin, R., Mills, N.L., 2017.  
558 Inhaled Nanoparticles Accumulate at Sites of Vascular Disease. *ACS Nano* 11, 4542–  
559 4552. <https://doi.org/10.1021/acsnano.6b08551>
- 560 Murros, K.E., Huynh, V.A., Takala, T.M., Saris, P.E.J., 2021. Desulfovibrio Bacteria Are  
561 Associated With Parkinson’s Disease. *Front. Cell. Infect. Microbiol.* 0.  
562 <https://doi.org/10.3389/fcimb.2021.652617>
- 563 Murugadoss, S., Lison, D., Godderis, L., Van Den Brule, S., Mast, J., Brassinne, F., Sebaihi,  
564 N., Hoet, P.H., 2017. Toxicology of silica nanoparticles: an update. *Arch. Toxicol.* 91,  
565 2967–3010. <https://doi.org/10.1007/s00204-017-1993-y>
- 566 Pereira, L.C., Pazin, M., Franco-Bernardes, M.F., Martins, A. da C., Barcelos, G.R.M.,  
567 Pereira, M.C., Mesquita, J.P., Rodrigues, J.L., Barbosa, F., Dorta, D.J., 2018. A  
568 perspective of mitochondrial dysfunction in rats treated with silver and titanium  
569 nanoparticles (AgNPs and TiNPs). *J. Trace Elem. Med. Biol.* 47, 63–69.  
570 <https://doi.org/10.1016/j.jtemb.2018.01.007>
- 571 Peters, R.J.B., Oomen, A.G., van Bommel, G., van Vliet, L., Undas, A.K., Munniks, S.,  
572 Bleys, R.L.A.W., Tromp, P.C., Brand, W., van der Lee, M., 2020. Silicon dioxide and  
573 titanium dioxide particles found in human tissues. *Nanotoxicology* 14, 420–432.  
574 <https://doi.org/10.1080/17435390.2020.1718232>
- 575 Prajitha, N., Athira, S.S., Mohanan, P.V., 2019. Bio-interactions and risks of engineered  
576 nanoparticles. *Environ. Res.* 172, 98–108.  
577 <https://doi.org/10.1016/j.envres.2019.02.003>
- 578 Pujalté, I., Dieme, D., Haddad, S., Serventi, A.M., Bouchard, M., 2017. Toxicokinetics of  
579 titanium dioxide (TiO<sub>2</sub>) nanoparticles after inhalation in rats. *Toxicol. Lett.* 265, 77–  
580 85. <https://doi.org/10.1016/j.toxlet.2016.11.014>
- 581 Rinninella, E., Cintoni, M., Raoul, P., Mora, V., Gasbarrini, A., Mele, M.C., 2021. Impact of  
582 Food Additive Titanium Dioxide on Gut Microbiota Composition, Microbiota-  
583 Associated Functions, and Gut Barrier: A Systematic Review of In Vivo Animal  
584 Studies. *Int. J. Environ. Res. Public Health* 18, 2008.  
585 <https://doi.org/10.3390/ijerph18042008>
- 586 Rogers, K.R., Navratilova, J., Stefaniak, A., Bowers, L., Knepp, A.K., Al-Abed, S.R., Potter,  
587 P., Gitipour, A., Radwan, I., Nelson, C., Bradham, K.D., 2018. Characterization of  
588 engineered nanoparticles in commercially available spray disinfectant products  
589 advertised to contain colloidal silver. *Sci. Total Environ.* 619–620, 1375–1384.  
590 <https://doi.org/10.1016/j.scitotenv.2017.11.195>
- 591 Rudramurthy, G.R., Swamy, M.K., 2018. Potential applications of engineered nanoparticles in  
592 medicine and biology: an update. *JBIC J. Biol. Inorg. Chem.* 23, 1185–1204.  
593 <https://doi.org/10.1007/s00775-018-1600-6>
- 594 Sikora, M., Stec, A., Chrabaszcz, M., Knot, A., Waskiel-Burnat, A., Rakowska, A.,  
595 Olszewska, M., Rudnicka, L., 2020. Gut microbiome in psoriasis: An updated review.  
596 *Pathogens* 9, 463.
- 597 Smith, J.R.H., Etherington, G., Shutt, A.L., Youngman, M.J., 2002. A study of aerosol  
598 deposition and clearance from the human nasal passage. *Ann. Occup. Hyg.* 46, 309–  
599 313.

- 600 Sutunkova, M.P., Solovyeva, S.N., Chernyshov, I.N., Klinova, S.V., Gurvich, V.B., Shur,  
601 V.Y., Shishkina, E.V., Zubarev, I.V., Privalova, L.I., Katsnelson, B.A., 2020.  
602 Manifestation of Systemic Toxicity in Rats after a Short-Time Inhalation of Lead  
603 Oxide Nanoparticles. *Int. J. Mol. Sci.* 21. <https://doi.org/10.3390/ijms21030690>
- 604 Tang, S., Zheng, J., 2018. Antibacterial Activity of Silver Nanoparticles: Structural Effects.  
605 *Adv. Healthc. Mater.* 7, e1701503. <https://doi.org/10.1002/adhm.201701503>
- 606 Umezawa, M., Onoda, A., Korshunova, I., Jensen, A.C.Ø., Koponen, I.K., Jensen, K.A.,  
607 Khodosevich, K., Vogel, U., Hougaard, K.S., 2018. Maternal inhalation of carbon  
608 black nanoparticles induces neurodevelopmental changes in mouse offspring. *Part.*  
609 *Fibre Toxicol.* 15, 36. <https://doi.org/10.1186/s12989-018-0272-2>
- 610 Vignal, C., Guilloteau, E., Gower-Rousseau, C., Body-Malapel, M., 2021. Review article:  
611 Epidemiological and animal evidence for the role of air pollution in intestinal diseases.  
612 *Sci. Total Environ.* 757, 143718. <https://doi.org/10.1016/j.scitotenv.2020.143718>
- 613 Wahle, T., Sofranko, A., Dekkers, S., Miller, M.R., Heusinkveld, H.J., Albrecht, C., Cassee,  
614 F.R., Schins, R.P.F., 2020. Evaluation of neurological effects of cerium dioxide  
615 nanoparticles doped with different amounts of zirconium following inhalation  
616 exposure in mouse models of Alzheimer's and vascular disease. *Neurochem. Int.* 138,  
617 104755. <https://doi.org/10.1016/j.neuint.2020.104755>
- 618 Wen, K., Tao, L., Tao, Z., Meng, Y., Zhou, S., Chen, J., Yang, K., Da, W., Zhu, Y., 2020.  
619 Fecal and Serum Metabolomic Signatures and Microbial Community Profiling of  
620 Postmenopausal Osteoporosis Mice Model. *Front. Cell. Infect. Microbiol.* 10, 535310.  
621 <https://doi.org/10.3389/fcimb.2020.535310>
- 622 Willing, B.P., Dicksved, J., Halfvarson, J., Andersson, A.F., Lucio, M., Zheng, Z., Järnerot,  
623 G., Tysk, C., Jansson, J.K., Engstrand, L., 2010. A pyrosequencing study in twins  
624 shows that gastrointestinal microbial profiles vary with inflammatory bowel disease  
625 phenotypes. *Gastroenterology* 139, 1844–1854.
- 626 Yin, I.X., Zhang, J., Zhao, I.S., Mei, M.L., Li, Q., Chu, C.H., 2020. The Antibacterial  
627 Mechanism of Silver Nanoparticles and Its Application in Dentistry. *Int. J.*  
628 *Nanomedicine* 15, 2555–2562. <https://doi.org/10.2147/IJN.S246764>
- 629 Zhai, Q., Li, T., Yu, L., Xiao, Y., Feng, S., Wu, J., Zhao, J., Zhang, H., Chen, W., 2017.  
630 Effects of subchronic oral toxic metal exposure on the intestinal microbiota of mice.  
631 *Sci. Bull.* 62, 831–840.
- 632

### 633 **Figure legends**

634

635 Fig. 1. (A) Transmission electron microscopic images and energy-dispersive X-ray spectra of  
636 typical nanoparticles from individual samples (Ag, SiO<sub>2</sub>, Ti, and TiO<sub>2</sub>). Scale bars represent  
637 100 nanometers. (B) Typical transmission electron microscopic images (backscattered electron  
638 detector for chemical contrast, secondary electron detector for morphological contrast) and  
639 elemental map of the nanoparticle mixture.

640

641 Fig. 2. The effects of inhalation of an engineered nanoparticle mixture (ENM) on male gut  
642 inflammatory status. Male mice were exposed to an airborne ENM consisting of Ag, SiO<sub>2</sub>, Ti,  
643 and TiO<sub>2</sub> or to control inhalation (CT; n=10/group). (A-B-C) Representative images of  
644 intestinal tissues (MGG staining; scale bar=100 μm) and inflammatory infiltration score in  
645 distal colon (A), proximal colon (B), and jejunum (C). (D-E-F) Quantification of mRNA levels  
646 of inflammatory cytokines by qRT-PCR in distal colon (D), proximal colon (E), and jejunum  
647 (F). \*=*p*<0.05, \*\*=*p*<0.01, \*\*\*=*p*<0.005, and \*\*\*\*=*p*<0.001 as determined by the Mann-  
648 Whitney U test.

649

650 Fig. 3. The effects of inhalation of an engineered nanoparticle mixture (ENM) on female gut  
651 inflammatory status. Female mice were exposed to an airborne ENM consisting of Ag, SiO<sub>2</sub>,  
652 Ti and TiO<sub>2</sub> or to control inhalation (CT; n=10/group). (A-B-C) Representative images of  
653 intestinal tissues (MGG staining; scale bar=100 μm) and inflammatory infiltration score in  
654 distal colon (A), proximal colon (B), and jejunum (C). (D-E-F) Quantification of mRNA levels  
655 of inflammatory cytokines by qRT-PCR in distal colon (D), proximal colon (E), and jejunum  
656 (F). \*=*p*<0.05, \*\*=*p*<0.01, and \*\*\*=*p*<0.005 as determined by the Mann-Whitney U test.

657

658 Fig. 4. The effects of inhalation of an engineered nanoparticle mixture (ENM) on male gut  
659 microbiota composition. Male mice were exposed to an airborne ENM consisting of Ag, SiO<sub>2</sub>,  
660 Ti, and TiO<sub>2</sub> or to control inhalation (CT; n=6/group). DNA was isolated from cecal content  
661 for MiSeq 16S ribosomal RNA gene sequencing. (A) Unweighted-uniFrac β-diversity index,  
662 \*\*\*=*p*<0.005 as determined by pairwise PERMANOVA. The relative abundance of bacteria  
663 was calculated based on amplicon sequence variants. (Bb) Overview of the relative abundance  
664 of gut bacteria depicted at the phylum level. The relative abundance of significantly changed

665 bacterial phyla (Bb'), classes (C), orders (D), and families (E).  $*=p<0.05$  as determined by the  
666 Mann-Whitney U test.

667

668 Fig. 5. The effects of inhalation of an engineered nanoparticle mixture (ENM) on female gut  
669 microbiota composition. Female mice were exposed to an airborne ENM consisting of Ag,  
670 SiO<sub>2</sub>, Ti, and TiO<sub>2</sub> or to control inhalation (CT; n=6/group). DNA was isolated from cecal  
671 content for MiSeq 16S ribosomal RNA gene sequencing. The relative abundance of bacteria  
672 was calculated based on amplicon sequence variants. (Aa) Overview of the relative abundance  
673 of gut bacteria depicted at the phylum level. The relative abundance of significantly changed  
674 bacterial phyla (Aa'), classes (B), orders (C), and families (D).  $*=p<0.05$  as determined by the  
675 Mann-Whitney U test.

676

677 Fig. 6. The effects of inhalation of an engineered nanoparticle mixture (ENM) on dextran  
678 sodium sulfate (DSS)-induced colitis development in males and females. Male and female mice  
679 were exposed to an airborne ENM consisting of Ag, SiO<sub>2</sub>, Ti, and TiO<sub>2</sub> (ENM) or to control  
680 inhalation (CT), and to a 2% DSS solution in drinking water in the last 6 days of the  
681 experimental protocol (n=10/group). (A) Male body weight variation during 6 days of DSS  
682 administration. (B) Male colon weight/size ratio. (C) Quantification of mRNA levels of  
683 inflammatory cytokines in male colon by qRT-PCR. (D) Female body weight variation during  
684 6 days of DSS administration. (E) Female colon weight/size ratio. (F) Quantification of mRNA  
685 levels of inflammatory cytokines in female colon by qRT-PCR.  $*=p<0.05$ ,  $**=p<0.01$ , and  
686  $****=p<0.001$  as determined by the Mann-Whitney U test.

687

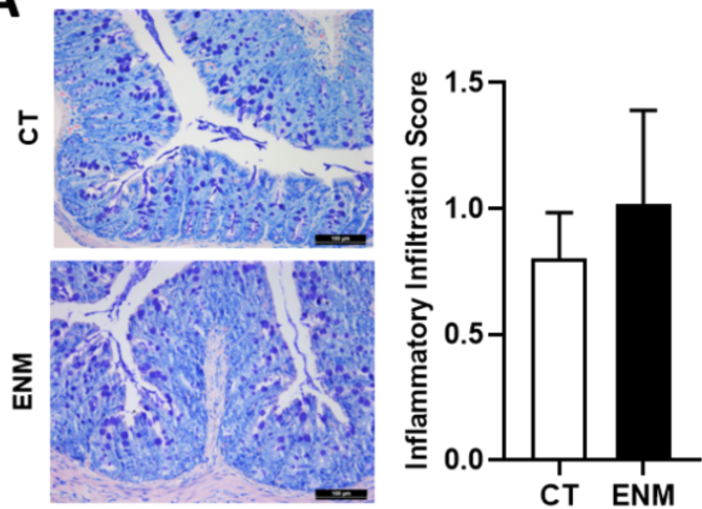
688 Fig. 7. The effects of the 4 engineered nanoparticles (EN) individually and in mixture on gut  
689 organoid inflammatory response. Quantification of mRNA levels of inflammatory cytokines

690 and alarmins by qPCR in inverted organoids treated with 0.02, 0.2, and 2  $\mu$ M of Ag, SiO<sub>2</sub>, Ti,  
691 TiO<sub>2</sub> EN, and the engineered nanoparticle mixture (ENM) after 24 h exposure (n=4/condition).  
692 Results are presented as fold change compared to untreated organoids. \*= $p$ <0.05 as determined  
693 by the Mann-Whitney U test.



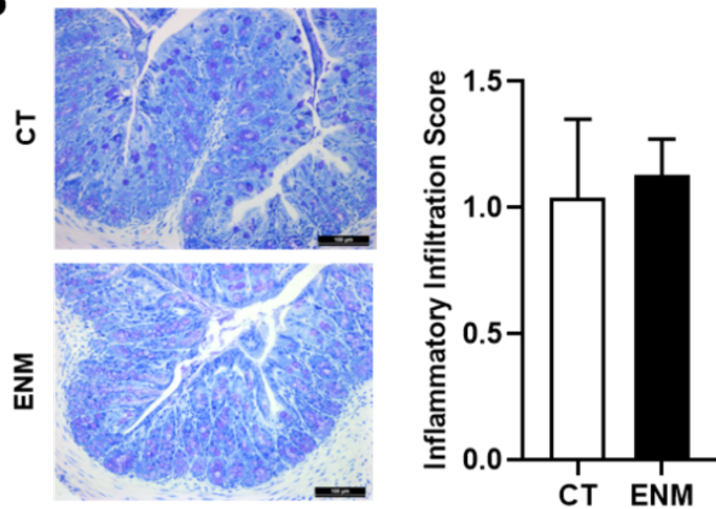
## Distal colon

**A**



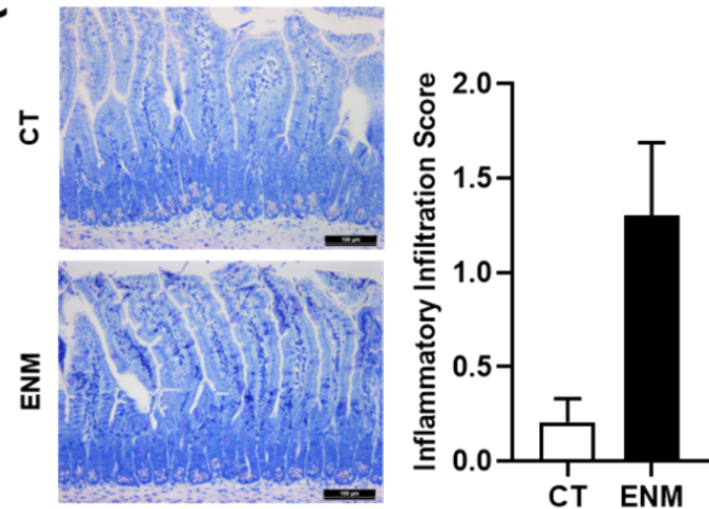
## Proximal colon

**B**

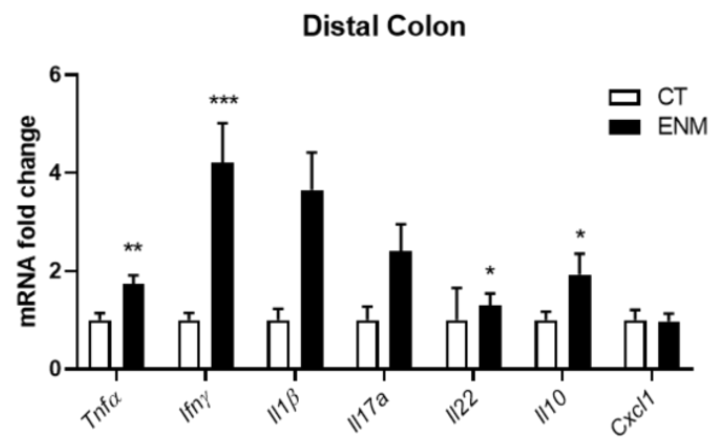


## Jejunum

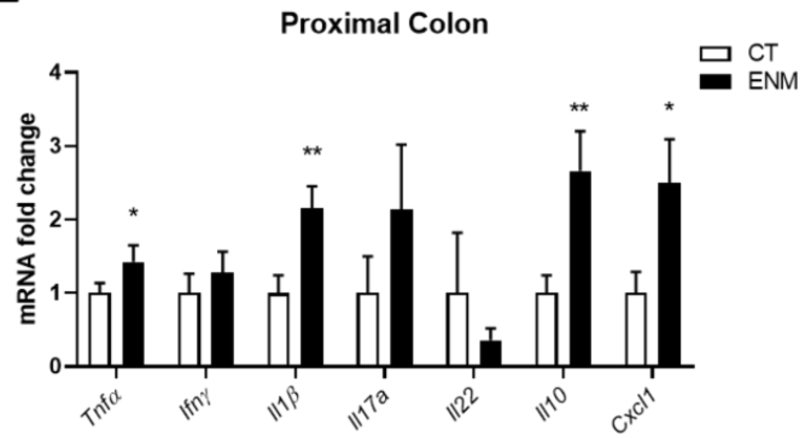
**C**



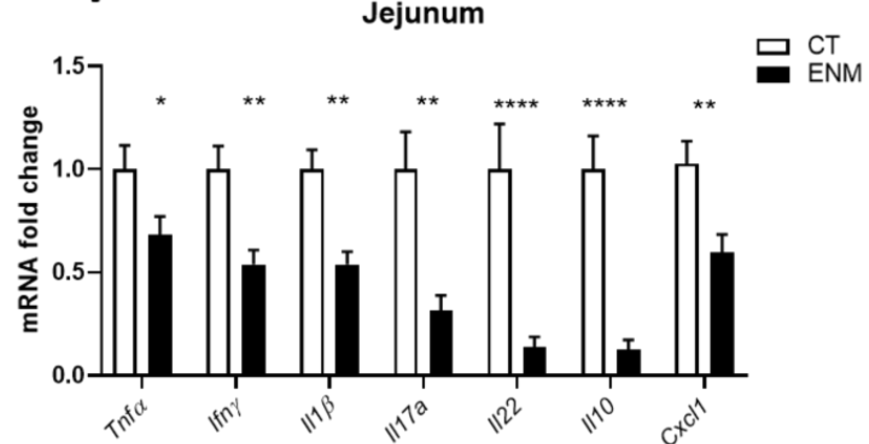
**D**



**E**

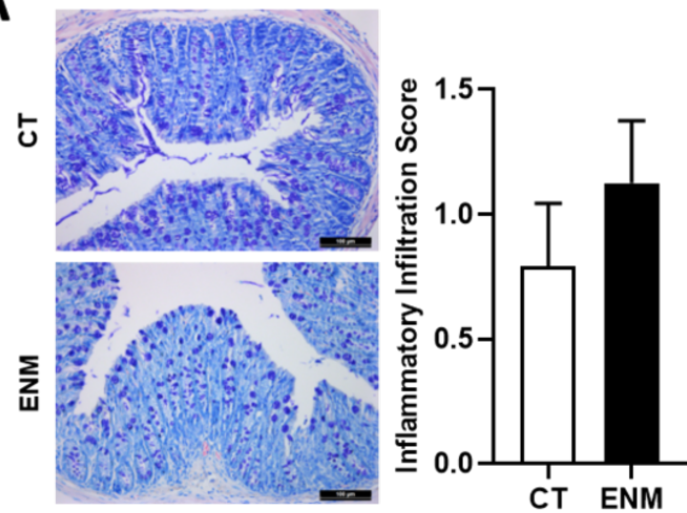


**F**



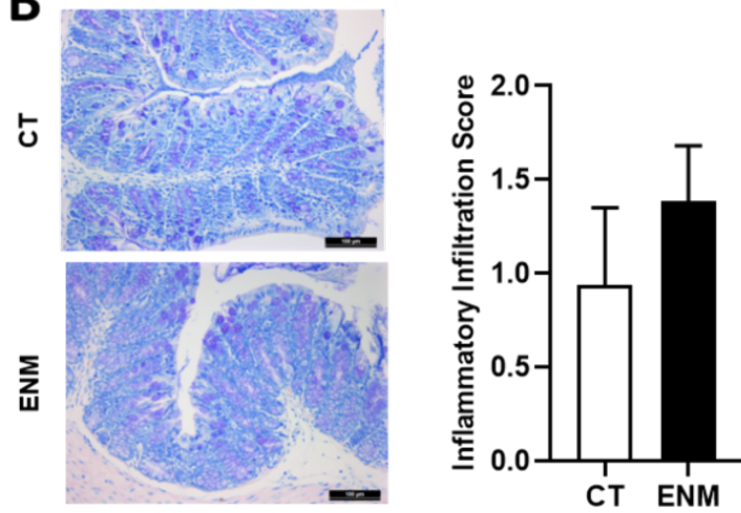
## Distal colon

**A**



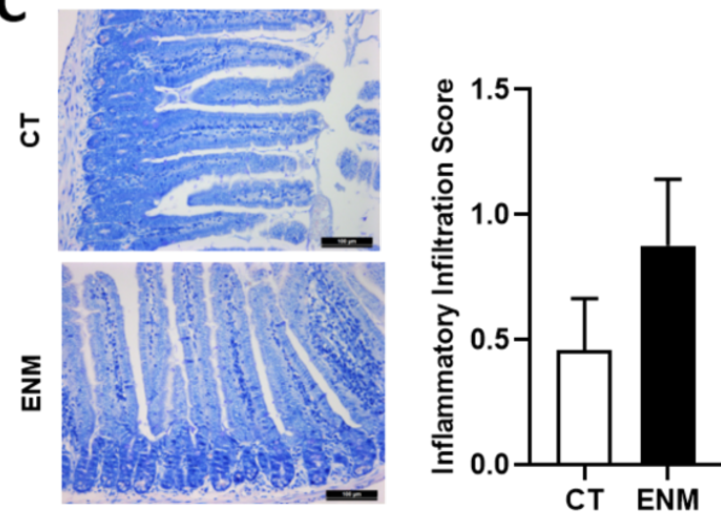
## Proximal colon

**B**

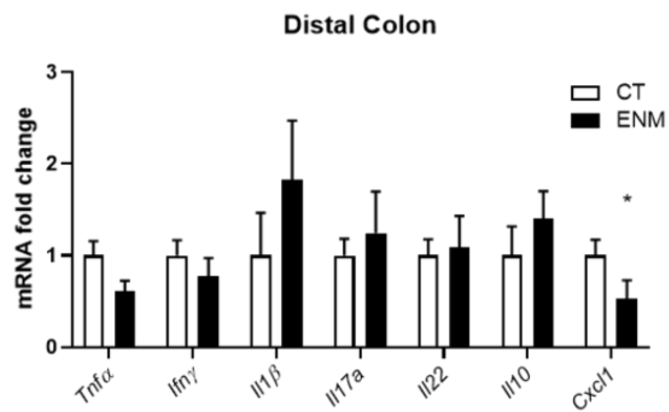


## Jejunum

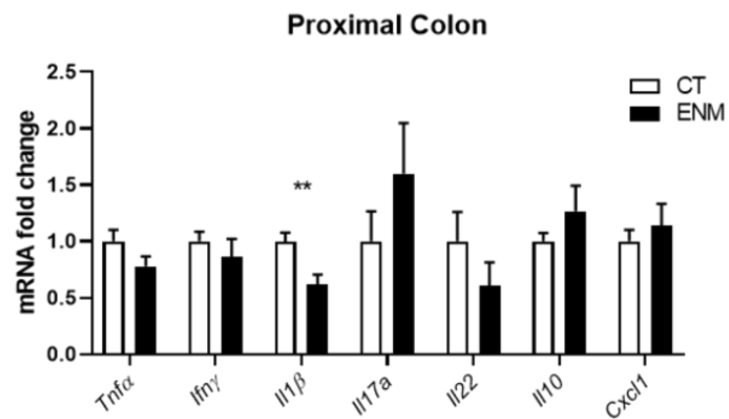
**C**



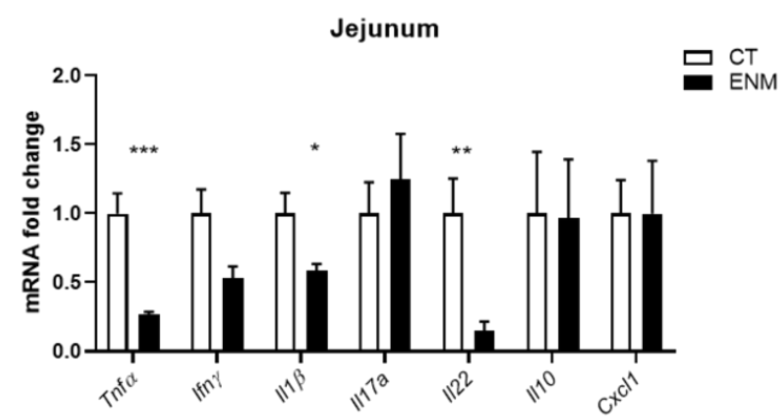
**D**

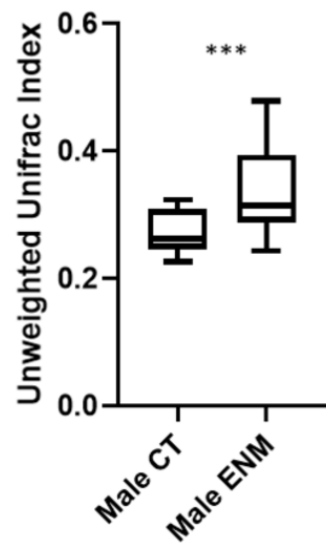
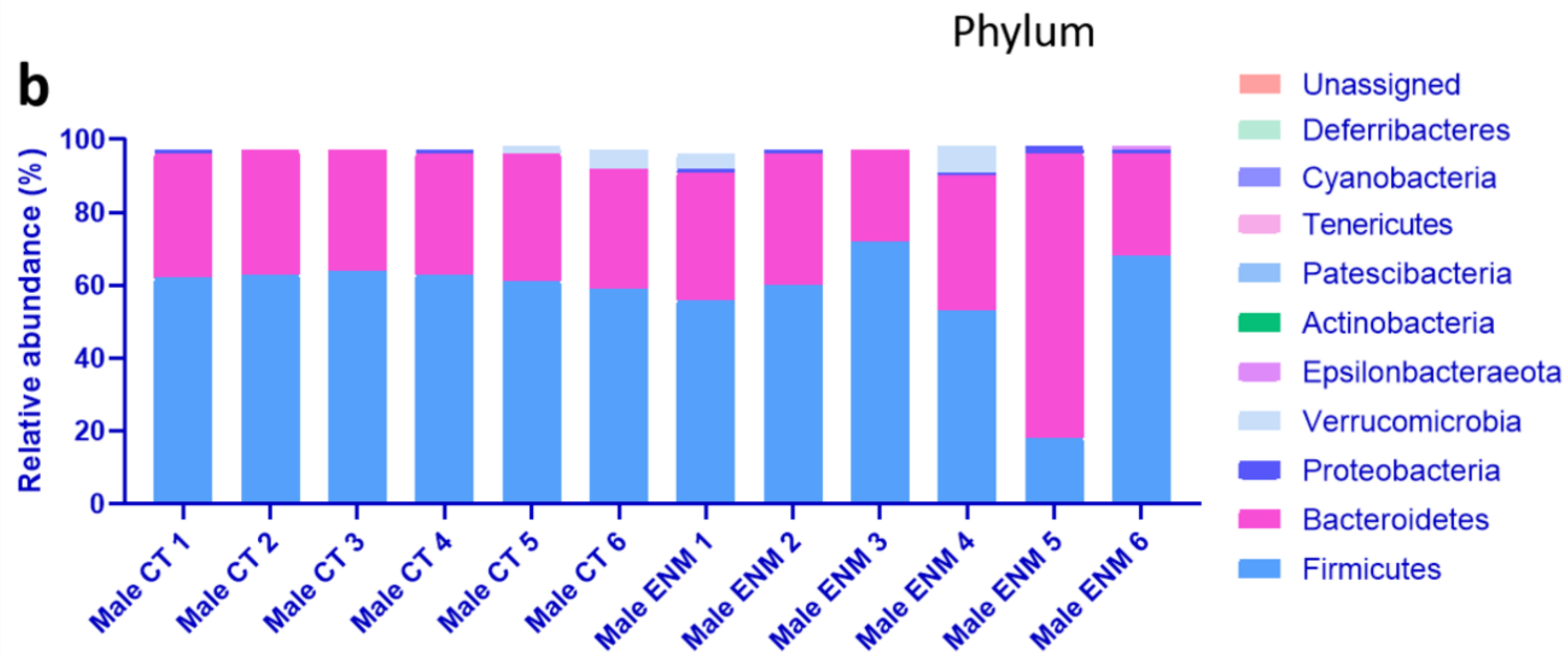
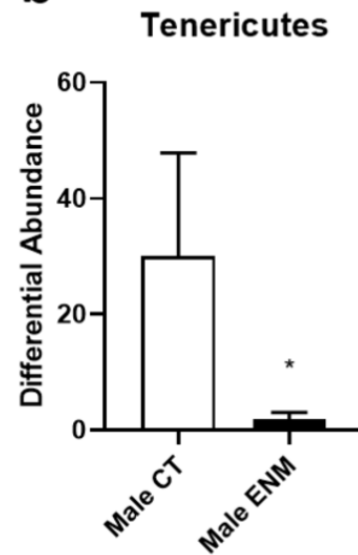
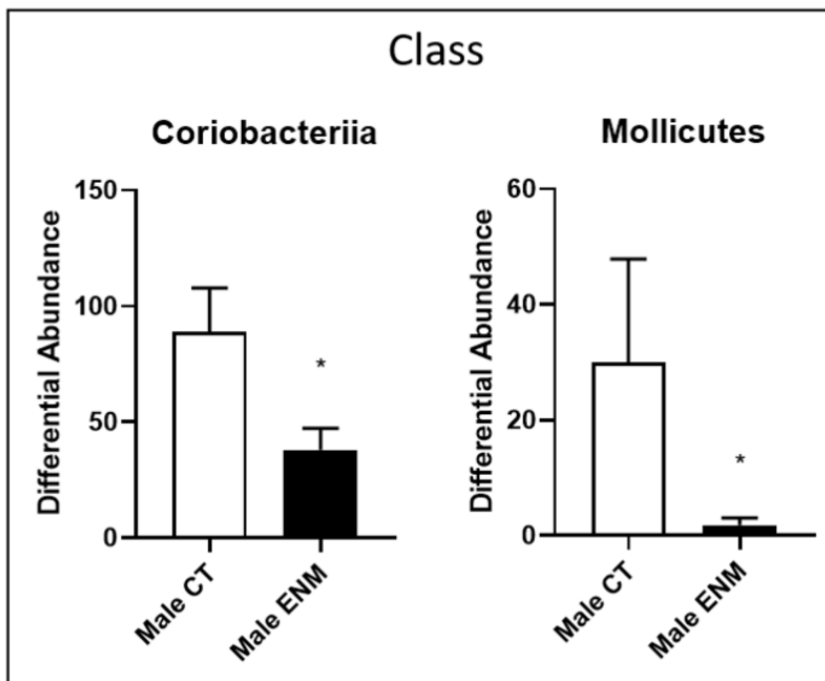
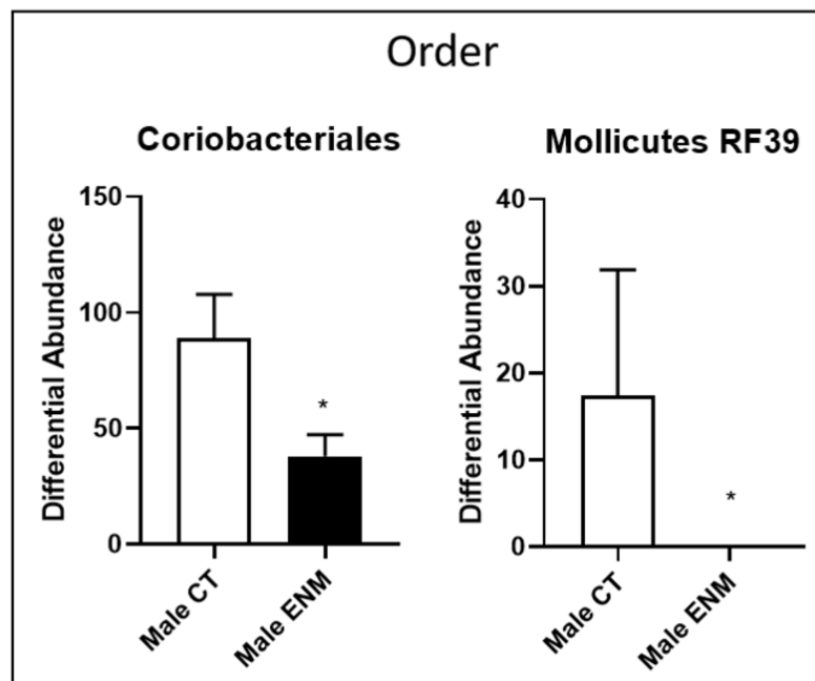
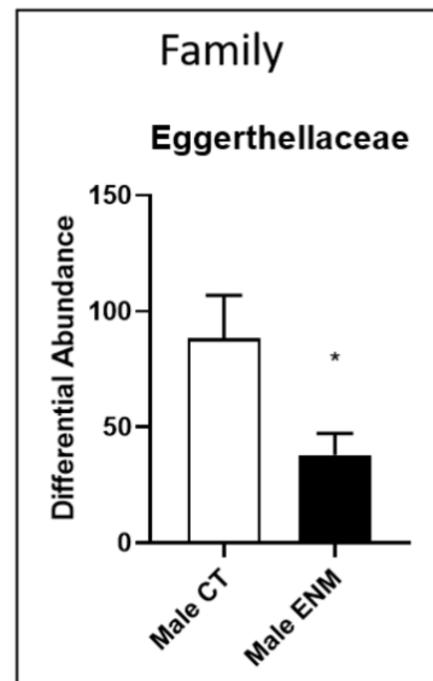


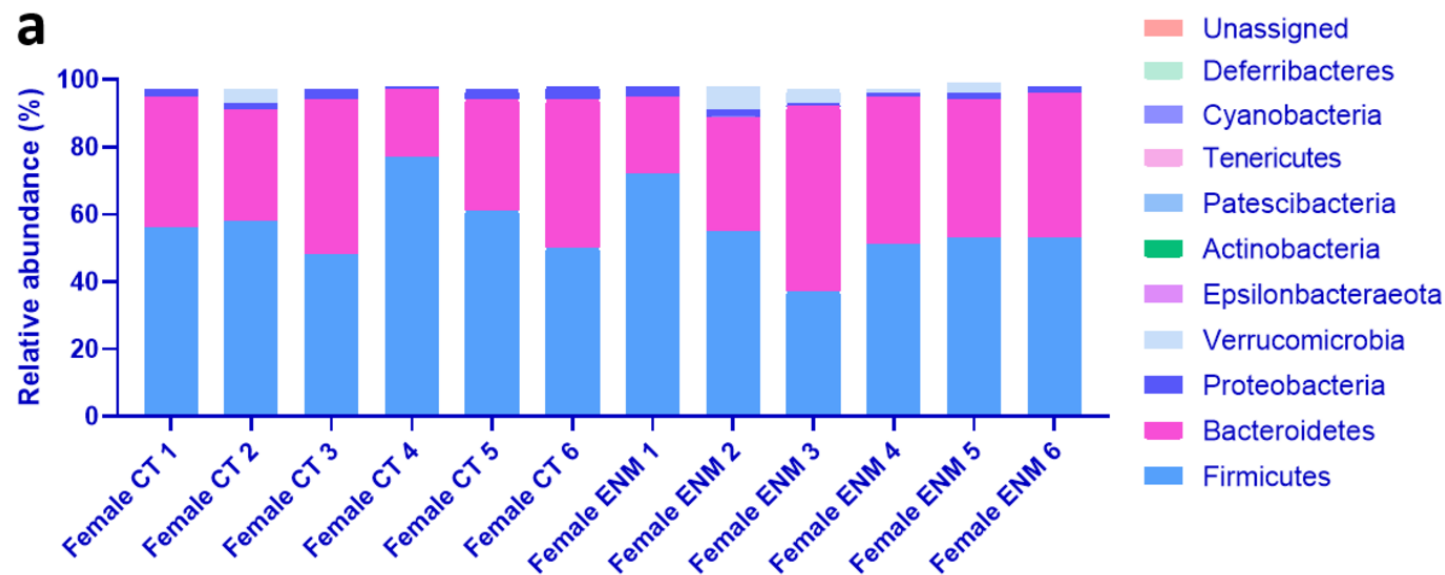
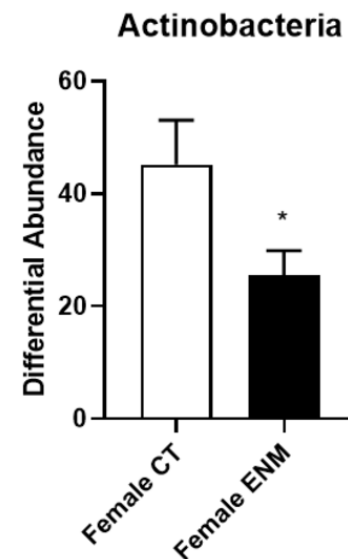
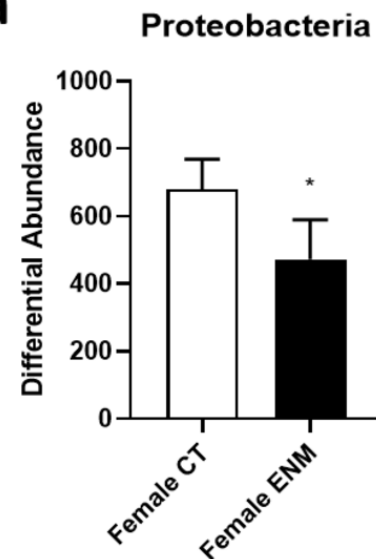
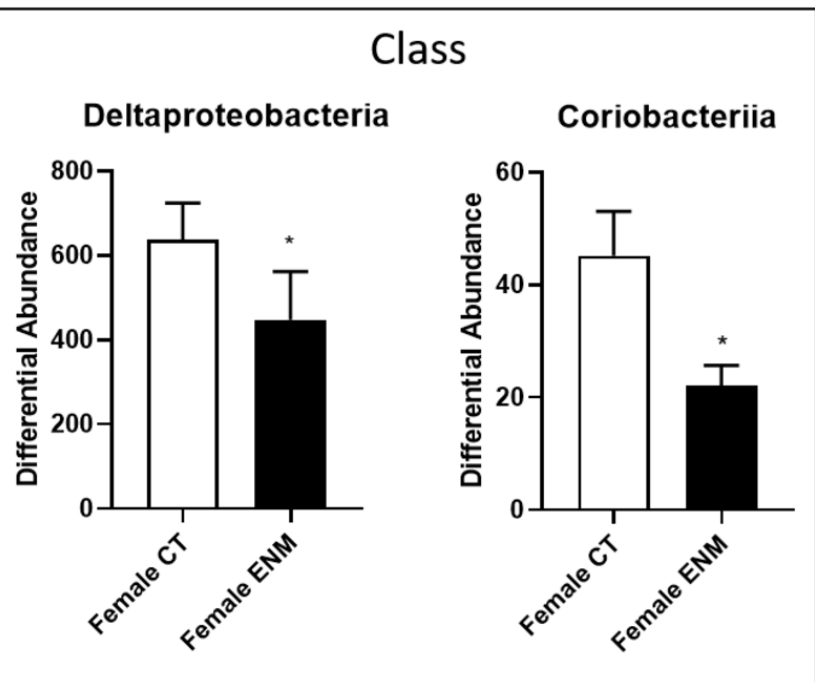
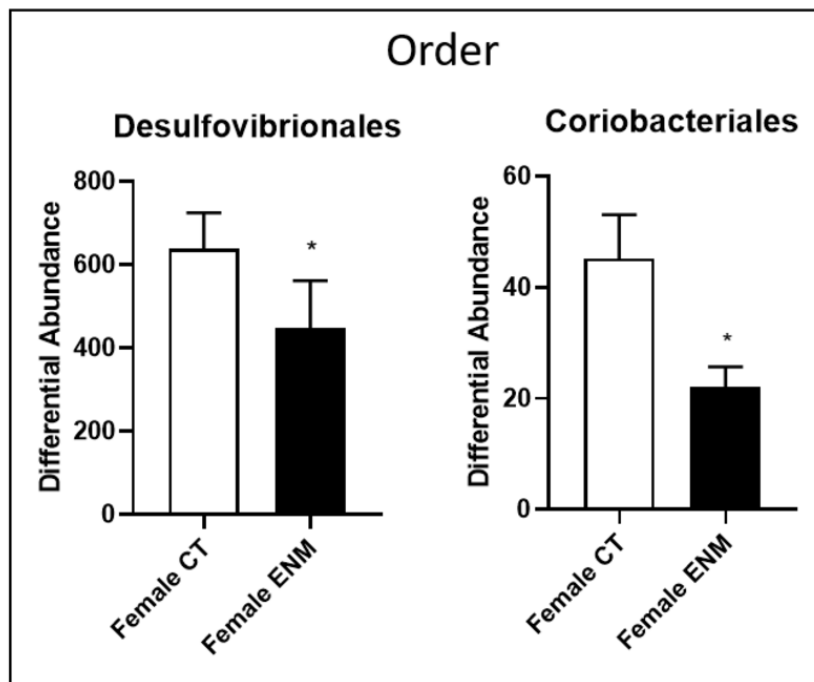
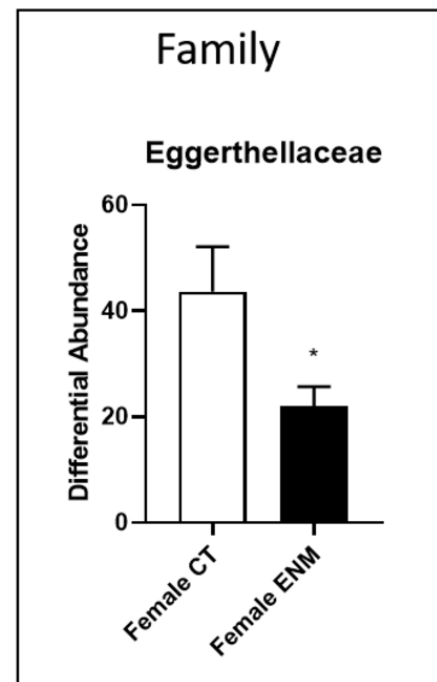
**E**

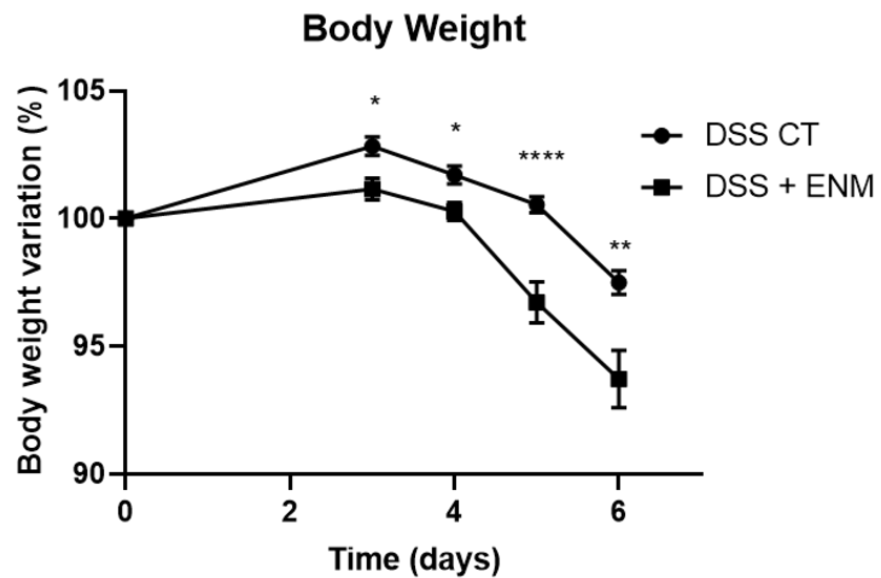
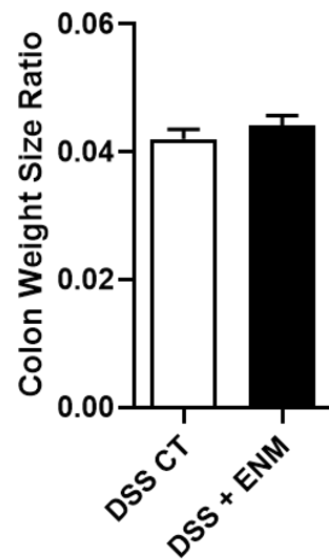
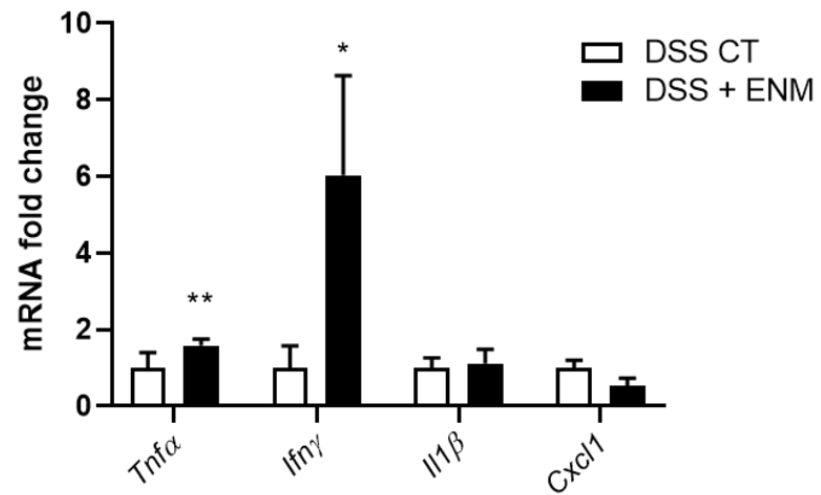
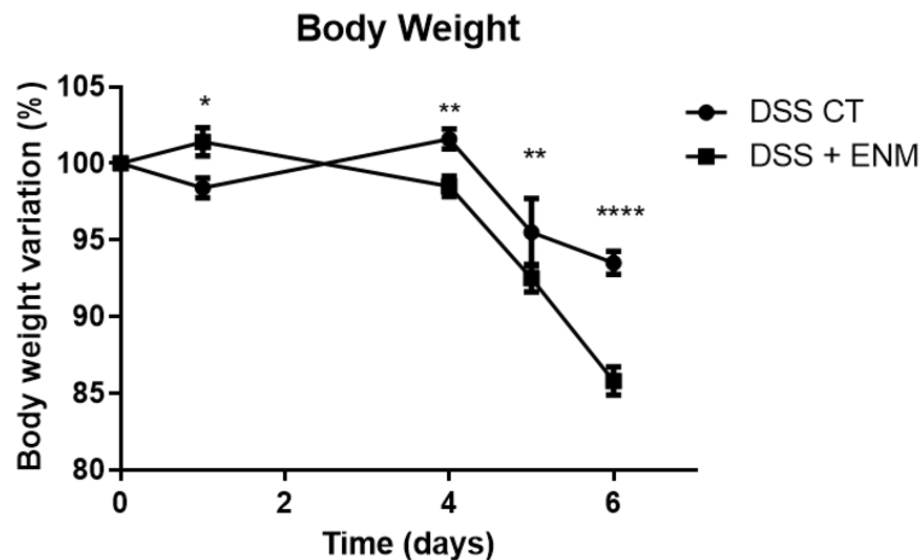
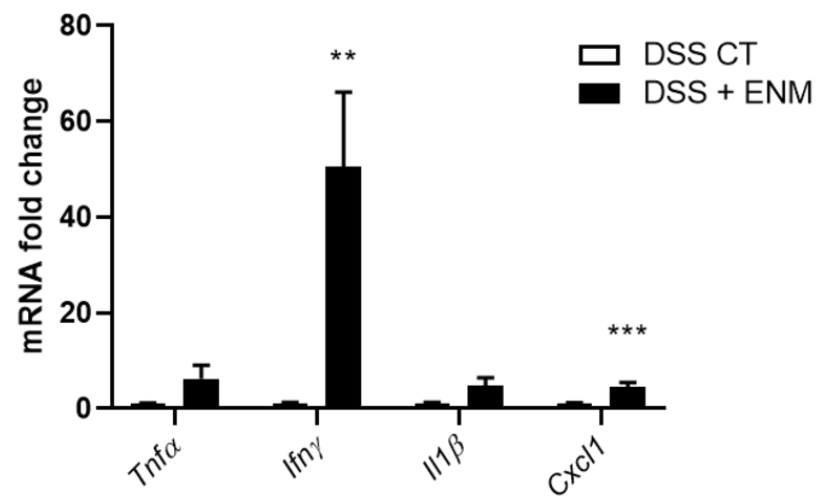


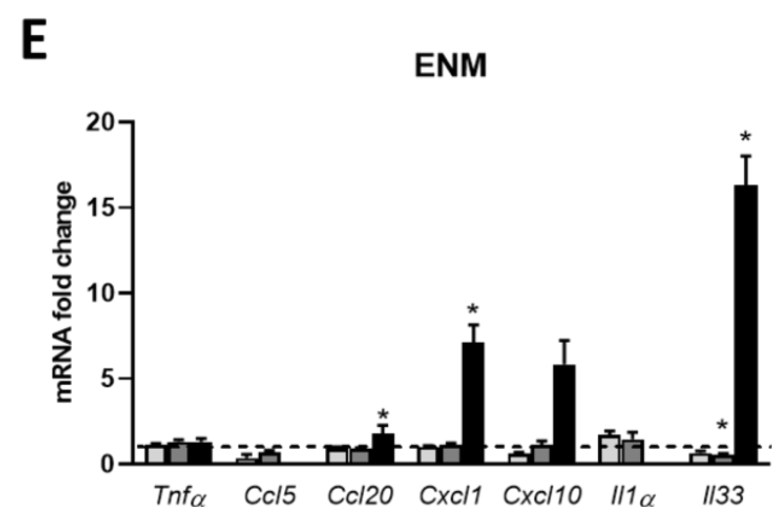
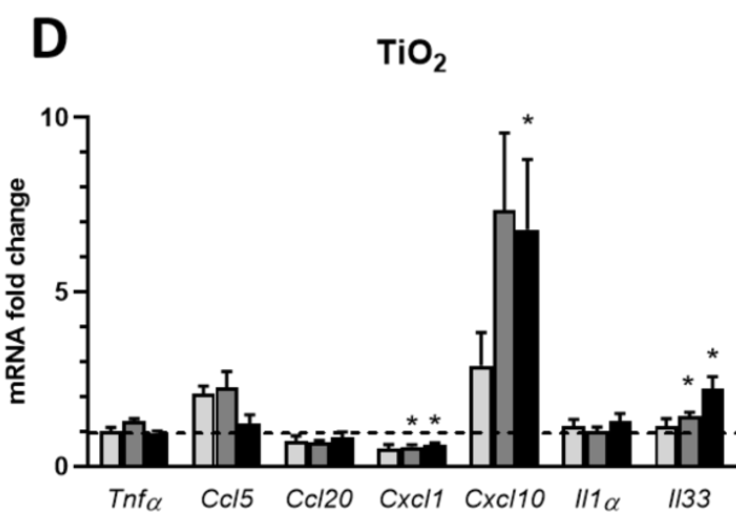
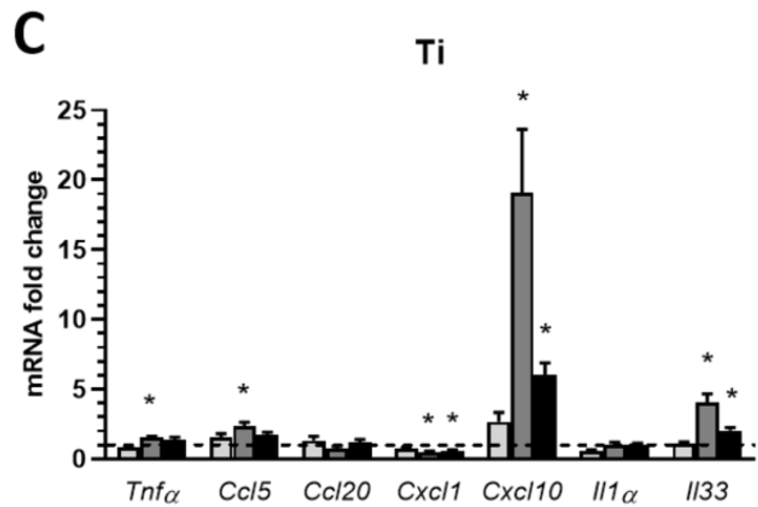
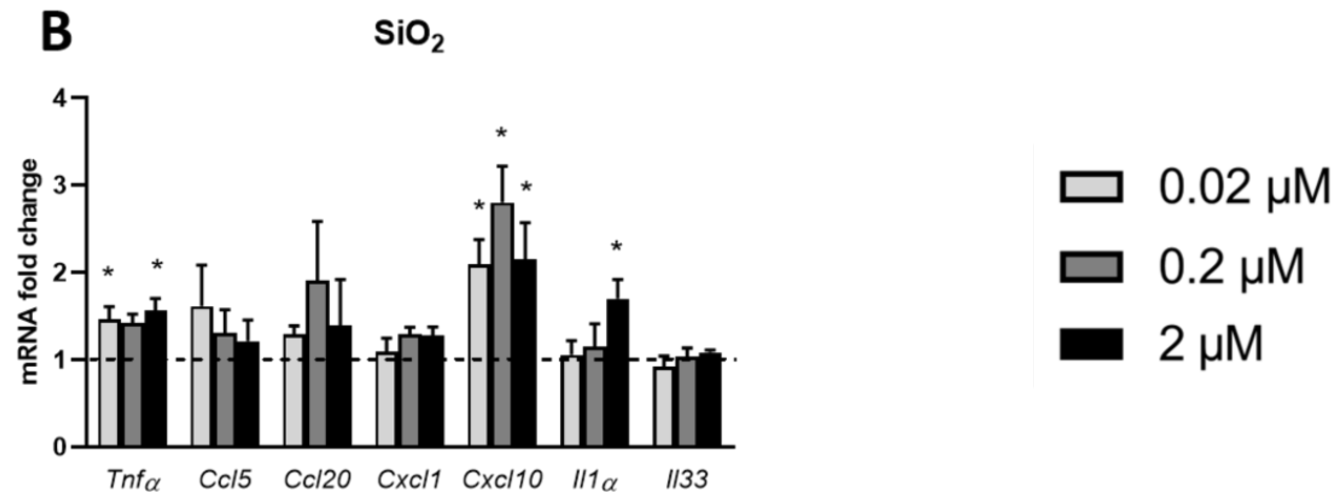
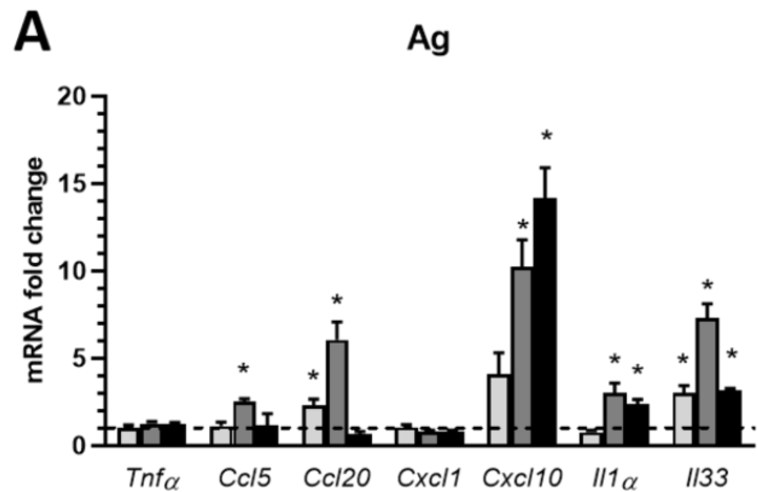
**F**



**A****B****b'****C****D****E**

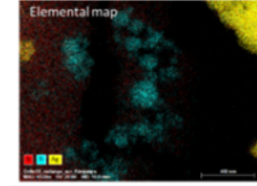
**A****a'****B****C****D**

**A****Males****B****C****D****Females****E****F**



# Exposure to atmospheric Ag, TiO<sub>2</sub>, Ti and SiO<sub>2</sub> engineered nanoparticles modulates inflammatory response and gut microbiota in mice

Most prevalent engineered nanoparticles in air:  
Silver (Ag), titanium dioxide (TiO<sub>2</sub>), titanium (Ti) and silicon dioxide (SiO<sub>2</sub>):  
gut adverse effects?



## 28-day inhalation in male and female mice

### Basal conditions

- Distal colon
- Proximal colon
- Jejunum



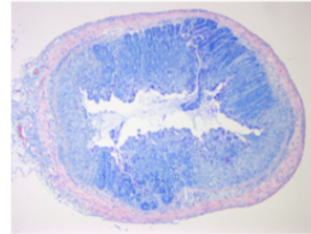
Tissue- and sex-dependent modulation of inflammatory cytokines

Gut microbiota



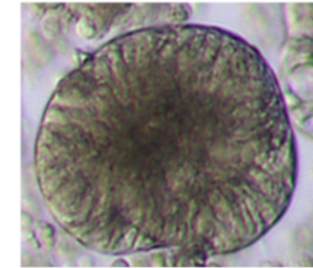
Sex-dependent and -independent modulation of bacterial composition

### Colitis



Worsening of colitis intensity

## Organoids



Engineered nanoparticle-specific modulation of cytokine and alarmin expression